The logarithmic phase singularity in the inverted harmonic oscillator

Cite as: AVS Quantum Sci. **4**, 024402 (2022); https://doi.org/10.1116/5.0074429
Submitted: 08 October 2021 • Accepted: 14 March 2022 • Published Online: 07 April 2022

Freyja Ullinger, Matthias Zimmermann and Wolfgang P. Schleich

AVS Quantum Science ARTICLE scitation.org/journal/aqs

The logarithmic phase singularity in the inverted harmonic oscillator

Cite as: AVS Quantum Sci. 4, 024402 (2022); doi: 10.1116/5.0074429
Submitted: 8 October 2021 · Accepted: 14 March 2022 ·
Published Online: 7 April 2022

Freyja Ullinger,[1,2] Matthias Zimmermann,[2] and Wolfgang P. Schleich[1,3]

AFFILIATIONS

[1]Institut für Quantenphysik and Center for Integrated Quantum Science and Technology (IQST), Universität Ulm, 89081 Ulm, Germany
[2]Institute of Quantum Technologies, German Aerospace Center (DLR), 89081 Ulm, Germany
[3]Hagler Institute for Advanced Study at Texas A&M University, Texas A&M AgriLife Research, Institute for Quantum Science and Engineering (IQSE) and Department of Physics and Astronomy, Texas A&M University, College Station, Texas 77843-4242, USA

ABSTRACT

A spacetime singularity is located at the center of a black hole and surrounded by an event horizon, separating spacetime into two disjunct regions: one of them accessible to an outside observer and one that is not. At the event horizon, a logarithmic phase singularity emerges in the mode functions of a massless scalar field, being characteristic for Hawking radiation emitted by the black hole. We demonstrate that related features are present in the elementary quantum system of an inverted harmonic oscillator. Central to our analysis are the energy eigenfunctions of this system and their phase space representation. At first glance, neither a horizon nor a logarithmic phase dependence are apparent. However, both features are hidden in phase space and revealed by a suitable coordinate transformation. In particular, we show that the Fourier transform of a logarithmic phase leads to an expression that is reminiscent of a specific quantum statistics, governing the reflection and transmission coefficients of the inverted harmonic oscillator.

I. INTRODUCTION

Intriguing physical phenomena manifest themselves in the proximity of singularities. Of particular interest are singularities induced by gravity, where spacetime itself becomes singular. In an outstanding work,[1] it has been demonstrated that a black hole, a particular spacetime singularity, is a robust prediction of general relativity.[2] Evidence for the existence of such a supermassive object at the center of the Milky Way has been provided by the exploration[3] of Sagittarius A*. Recently, gravitational wave detection has even enabled the first observation[4] of a merging binary black hole system.

However, due to their weak nature, unobserved so far are quantum effects that cause a thermal evaporation of black holes. At the very heart of this so-called Hawking radiation[5] lies a *logarithmic phase singularity* that manifests itself at the event horizon encoded in the metric of spacetime. Its origins are to be found in the hyperbolic motion in curved spacetime.[6]

There are many situations when physical systems display phenomena connected to black hole evaporation.[7] Arguably, the most prominent example is acceleration radiation,[8] as suggested by Unruh, which is related to Hawking radiation via the equivalence principle. However, even two-level atoms falling into a black hole would emit acceleration radiation which resembles, but is different from, Hawking radiation for a distant observer. Also, here, a logarithmic phase singularity appears in combination with an event horizon, resulting in a particular form of the excitation probability of the atoms.[9–11] Related features emerge in the context of quantum chaos,[12] the quantum Hall effect,[13,14] and the Riemann Zeta function.[15]

By now, various systems analogous to black holes have been identified[16,17] that are experimentally accessible and enable a direct study of the phenomena noted above. They range from the presence of a sonic horizon for sound waves,[18] over the field of optics,[19] as expressed in the quantum catastrophe of slow light,[20,21] and Bose– Einstein condensates,[22–24] to setups employing water waves.[25,26]

Insight into this plethora of physical systems can be provided by simple models that cover the main features of the underlying effects. In the view of Hawking radiation, such an elementary model[12,13,27,28] is the inverted harmonic oscillator.[29–33] We point out that the analogy of both systems has already been studied in detail in Ref. 13. In

contrast to this work, we take a different viewpoint and focus on a quantum mechanical perspective that becomes most evident within a phase space formulation. By providing an in-depth analysis of the inverted harmonic oscillator, we concentrate on the key ingredients of the apparent similarities in both systems. We trace them back to the presence of horizons and a logarithmic phase singularity.

In our article, we present a detailed study of a particle exposed to an inverted parabolic potential. By providing a short review, we relate relevant phenomena of quantum field theory such as Hawking radiation to this simple quantum system. Similar as the event horizon of a black hole separates spacetime into two disjunct regions, the inverted harmonic oscillator also displays horizons, which are now located in phase space. These horizons, appearing already in the classical dynamics of a particle subject to an inverted parabolic potential, crucially influence the corresponding quantum mechanical situation. In fact, this feature becomes most evident in Wigner phase space, which provides an overall and intuitive picture of the problem. By deriving the Wigner functions of the energy eigenstates, we demonstrate that they only live on a half plane of phase space that is isolated by a horizon.

However, it is surprising that the position representation of the energy eigenstates does not display such a horizon. We show that only by choosing a particular representation, the horizons can be recovered. In these rotated quadratures, the quantum waves are governed by a logarithmic phase singularity in combination with an amplitude singularity. We argue that the occurrence of a logarithmic phase singularity is of central relevance in establishing a connection between this system and the evaporation of a black hole. Indeed, the mode function of a massless scalar field also displays a logarithmic phase singularity at the event horizon of a black hole.

Moreover, it is the Fourier transform of this mode function that leads to the appearance of a Bose–Einstein statistics that governs the number of particles emitted by a black hole.[27,34,35] While this is a result of the second quantization of a scalar field, a related dependency arises in the single particle problem of an inverted harmonic oscillator. Indeed, the transmission and reflection coefficients of the inverted harmonic oscillator resemble a Fermi–Dirac distribution.[29,30,36] We demonstrate that this dependency results from the Fourier transform of a logarithmic phase singularity in combination with an amplitude singularity that arises at a horizon in phase space.

With the help of an elementary quantum system, our analysis thus reveals underlying effects of Hawking radiation. We hope that our results might stimulate further research into this direction and allow us to connect at first glance seemingly unrelated fields.

Our article is structured as follows. Section II provides a short overview on pair production in the presence of an electric field and the evaporation of a black hole. It serves the purpose to establish a link of these quantum effects to the system of the inverted harmonic oscillator. In Sec. III, we concentrate on the inverted harmonic oscillator in the classical domain. In particular, we present the emergence of horizons in phase space and the origin of the logarithmic singularity. Next, we turn to the quantum domain in Sec. IV. Here, we address the singularities present in the energy eigenfunctions of the inverted harmonic oscillator. We establish the relation to features familiar from Hawking radiation emitted at the event horizon of a black hole. Especially, we show that a logarithmic phase singularity in combination with an amplitude singularity leads to a distribution that resembles the Fermi–Dirac statistics. In Sec. V, we illustrate our results in phase space. For this purpose, we make use of Wigner functions corresponding to the energy eigenstates of the inverted harmonic oscillator. Due to the presence of horizons, these functions only live on a half plane of phase space. We conclude in Sec. VI by summarizing our results and provide an outlook to future topics of interest.

Our analysis is supplemented by two Appendixes which contain transformations between different basis states as employed for the description of the inverted harmonic oscillator. In Appendix A, we focus on the position representation of rotated quadrature states. In Appendix B, we derive the position representation of the energy eigenstates.

II. MODELING EFFECTS OF QUANTUM FIELD THEORY

In the following, we review two quantum field effects. In particular, we consider the pair production induced by the presence of a static electric field and the emission of Hawking radiation at the event horizon of a black hole. We focus on the singularities encoded in the mode functions for these problems and establish a relation to the simple quantum system of an inverted harmonic oscillator.

A. Pair production due to a static electric field

In the early days of quantum mechanics, it has already been argued that an electric field changes the vacuum in such a way that pairs of particles and antiparticles can be created.[37,38] In order to obtain a deeper insight into this mechanism, we relate this problem to the system of an inverted harmonic oscillator, which is at the heart of our article.

For the sake of simplicity, we restrict ourselves to one spatial dimension x and follow the approach presented in Refs. 7 and 39 for the case of a scalar field Ψ. In the presence of a constant electric field $\mathscr{E}$, the Klein–Gordon equation takes the form

$$\left[\left(\frac{1}{c}\frac{\partial}{\partial t}-\mathrm{i}\frac{q\mathscr{E}}{\hbar c}x\right)^2-\frac{\partial^2}{\partial x^2}\right]\Psi=-\left(\frac{mc}{\hbar}\right)^2\Psi, \tag{1}$$

where m and q are the mass and charge, respectively, c is the speed of light, and $\hbar$ denotes the reduced Planck constant.

Next, due to the stationary nature of the electric field $\mathscr{E}$, we identify solutions of Eq. (1) by separating the dependence of $\Psi=\Psi(t,x)$ with regard to time t and position x. For a mode $\Psi_\Omega(t,x)=\exp(-\mathrm{i}\Omega t)f_\Omega(x)$ of frequency Ω, the mode function $f_\Omega(x)$ then satisfies the equation

$$\left[-\frac{\hbar^2}{2m}\frac{\partial^2}{\partial x^2}-\frac{1}{2}m\omega^2(x-x_0)^2\right]f_\Omega(x)=\hbar\omega\varepsilon f_\Omega(x) \tag{2}$$

resulting from Eq. (1). Here, we have introduced the parameters $\omega\equiv q\mathscr{E}/(mc)$, $x_0=-\hbar\Omega/(q\mathscr{E})$, and $\varepsilon=-mc^2/(2\hbar\omega)$.

It is intriguing to ascertain that Eq. (2) actually corresponds to the stationary Schrödinger equation of a quantum particle of mass m. This particle is exposed to a one-dimensional inverted harmonic oscillator of steepness ω which is centered at the coordinate x_0. As a consequence, the mode function $f_\Omega(x)$ coincides with the eigenfunction of energy $\hbar\omega\varepsilon$ of an inverted harmonic oscillator.

In the succeeding Secs. III and IV, we demonstrate that the behavior of these eigenfunctions is governed by horizons in phase

space at which a logarithmic phase singularity occurs. For this reason, we anticipate that a better understanding of an inverted harmonic oscillator might lead to a deeper insight into the pair creation in the presence of a strong electric field.

B. Hawking radiation

In the following, we show that not only the pair creation mechanism but also the evaporation of a black hole displays analogies to the inverted harmonic oscillator. For this purpose, we consider a scalar quantum field with massless quanta in the presence of the gravitational field of a static, uncharged, and homogeneous black hole of mass M. For further details, we refer to Refs. 7 and 13.

The modes of the scalar field ψ can be obtained by solving the covariant Klein–Gordon equation

$$\frac{1}{\sqrt{-g}}\partial_\mu g^{\mu\nu}\sqrt{-g}\partial_\nu\psi = 0, \tag{3}$$

where $g = \det(g^{\mu\nu})$ denotes the determinant of the metric tensor $g^{\mu\nu}$.

We analyze the field in the Schwarzschild space, that is for the radius $r > r_s$, where the Schwarzschild radius $r_s = 2GM/c^2$ determines the event horizon of the black hole in terms of the gravitational constant G and the speed of light c. In this domain, spacetime is governed by the Schwarzschild metric with the line element

$$g_{\mu\nu}\mathrm{d}x^\mu\mathrm{d}x^\nu = -c^2\left(1-\frac{r_s}{r}\right)\mathrm{d}t^2 + \frac{1}{1-\frac{r_s}{r}}\mathrm{d}r^2 + r^2\mathrm{d}\Omega_s^2. \tag{4}$$

Here, $\mathrm{d}\Omega_s^2 = \mathrm{d}\theta^2 + \sin^2\theta\mathrm{d}\phi^2$ denotes the square of the differential for the solid angle Ω_s as determined by the polar angle θ and the azimuthal angle ϕ in spherical coordinates.

Next, we introduce the Regge–Wheeler tortoise coordinate

$$r^* = r + r_s\ln\left|1-\frac{r}{r_s}\right| \tag{5}$$

with

$$\frac{\mathrm{d}r^*}{\mathrm{d}r} = \frac{1}{1-\frac{r_s}{r}} \tag{6}$$

such that the line element in Eq. (4) simplifies to

$$g_{\mu\nu}\mathrm{d}x^\mu\mathrm{d}x^\nu = \left(1-\frac{r_s}{r}\right)(-c^2\mathrm{d}t^2 + \mathrm{d}r^{*2}) + r^2\mathrm{d}\Omega_s^2. \tag{7}$$

By making use of the determinant $g = -1/(r^4\sin^2\theta)$ of the metric tensor $g^{\mu\nu}$, we recast the Klein–Gordon equation (3) as[7]

$$\frac{1}{r-r_s}\left[-\frac{1}{c^2}\frac{\partial^2}{\partial t^2} + \frac{\partial^2}{\partial r^{*2}} + \left(1-\frac{r_s}{r}\right)\left(\frac{r_s}{r^3} - \frac{\hat{\mathbf{L}}^2}{\hbar^2 r^2}\right)\right] r\psi = 0, \tag{8}$$

where we have introduced the angular momentum operator $\hat{\mathbf{L}}$.

For spherical symmetric waves with angular momentum quantum number $l = 0$, we arrive at

$$\left(-\frac{1}{c^2}\frac{\partial^2}{\partial t^2} + \frac{\partial^2}{\partial r^{*2}}\right) r\psi_0 = 0 \tag{9}$$

for $r \approx r_s$, where the last term in Eq. (8) can be neglected.

The separation of variables $\psi_0(t,r) = q(t)R_0(r)$ in Eq. (9) then yields the relation

$$\frac{1}{c^2}\frac{\partial_t^2 q(t)}{q(t)} = \frac{\partial_{r^*}^2[rR_0(r)]}{rR_0(r)}. \tag{10}$$

Thus, in the temporal domain, we obtain the oscillator equation

$$\left(\frac{\partial^2}{\partial t^2} + \Omega^2\right) q(t) = 0 \tag{11}$$

for the function $q(t)$, and in radial direction, we arrive at

$$\left(\frac{\partial^2}{\partial r^{*2}} + k^2\right) rR_0(r) = 0 \tag{12}$$

for $R_0(r)$ with $k = \Omega/c$.

The radial equation (12) then determines the mode functions

$$R_{0,k}^{\pm}(r) = \frac{\mathrm{e}^{\pm\mathrm{i}kr^*}}{r} = \frac{1}{r}\mathrm{e}^{\pm\mathrm{i}k\left(r + r_s\ln\left|1-\frac{r}{r_s}\right|\right)}, \tag{13}$$

which display a *logarithmic phase singularity* at the event horizon located at $r = r_s$. Here, we have made use of the relation between the tortoise coordinate r^* and the radial coordinate r presented in Eq. (5). In addition, the occupation of a mode relies on the quantization of the time-dependent Eq. (11), leading to the appearance of the creation and annihilation operators that are familiar from the harmonic oscillator.

The logarithmic singularity in Eq. (13) plays a crucial role in the case of a two-level atom falling into a black hole and emitting acceleration radiation.[10] There it has been shown that it is the *Fourier transform* of the *logarithmic phase* that determines the excitation probability such that it follows a *Bose–Einstein distribution*.

In the case of Hawking radiation,[5] the pair creation at the event horizon of a black hole is described in terms of a scattering problem for ingoing and outgoing waves. However, it is the Fourier transform of the logarithmic phase in the mode functions that determines the number of particles emitted in a mode of frequency Ω as

$$f(\Omega) = \frac{1}{\mathrm{e}^{2\pi\Omega/\kappa} - 1} \tag{14}$$

times the number of particles that would have been absorbed. Here, κ denotes the surface gravity of the black hole. Clearly, Eq. (14) corresponds to a Bose–Einstein statistics.

To conclude, the relationship of the pair creation mechanism and the evaporation of a black hole to the system of the inverted harmonic oscillator might reveal a deeper insight into both phenomena. In the following, we demonstrate this relationship with the help of a detailed analysis of the inverted harmonic oscillator.

III. CLASSICAL FEATURES OF THE INVERTED HARMONIC OSCILLATOR

As counterpart of the harmonic oscillator, the inverted harmonic oscillator[13,29–33] has found great application in modeling systems that display a point of instability. For instance, it has been applied in the context of nuclear fission[40,41] or to explore dissipative quantum systems with a potential barrier.[42] Yet, many interesting features have not been analyzed to the same extent as those emerging in the harmonic oscillator.

In the following, we focus on the dynamics of a classical particle in the presence of an inverted harmonic oscillator potential. We identify horizons in phase space in combination with a logarithmic singularity. Our findings provide the basis for the analysis of the corresponding quantum effects.

A. Emergence of the horizons in phase space

A *classical particle* of mass m exposed to the parabolic potential $V(x) \equiv -(1/2)m\omega^2 x^2$ is described by the Hamiltonian

$$H(x,p) = \frac{p^2}{2m} - \frac{1}{2}m\omega^2 x^2 \tag{15}$$

characterizing an inverted harmonic oscillator of steepness ω, as depicted in Fig. 1(a). Here, p denotes the momentum and x is the position.

Accordingly, the dynamics of the particle is governed by the Hamilton equations of motion

$$\dot{x} = \frac{\partial H}{\partial p} = \frac{p}{m}, \tag{16}$$

$$\dot{p} = -\frac{\partial H}{\partial x} = m\omega^2 x, \tag{17}$$

whose solution gives raise to the classical phase space trajectories

$$x_{\rm cl}(t) = x_0 \cosh(\omega t) + \frac{p_0}{m\omega}\sinh(\omega t), \tag{18}$$

$$p_{\rm cl}(t) = m\omega x_0 \sinh(\omega t) + p_0 \cosh(\omega t), \tag{19}$$

with x_0 and p_0 being the initial position and momentum at time $t = 0$, respectively.

Since the Hamiltonian $H(x, p)$, Eq. (15), is time-independent, each phase space trajectory is associated with a particular energy $E = H(x_0, p_0)$ as determined by the initial condition for the respective motion. Due to the quadratic dependence on x and p, the Hamiltonian $H(x, p)$ is invariant[31] under the transformations (i) $p \to -p$ and (ii) $x \to -x$. Hence, there are *two* distinct motions corresponding to the same value of the energy E, which however differ by the incoming direction of the particles as shown in Fig. 1. For negative energies $E < 0$ (red and orange), the particle is reflected at the potential barrier, while for positive energies $E > 0$ (blue and green), the particle is transmitted.

In Fig. 1(b), we present the corresponding dynamics in phase space by the hyperbolas $\{x_{\rm cl}(t), p_{\rm cl}(t)\}$ for different initial conditions x_0 and p_0 according to Eqs. (18) and (19). For each trajectory associated with an incoming particle from the left of energy $E < 0$ (red) and $E > 0$ (blue), there is an equivalent trajectory for an incoming particle from the right with energy $E < 0$ (orange) and $E > 0$ (green), respectively. For negative energies $E < 0$, the motion of the particle is restricted to the domain $x < 0$ (incoming from the left) or $x > 0$ (incoming from the right). For positive energies $E > 0$, its motion is instead restricted to the domain $p > 0$ (incoming from the left) and $p < 0$ (incoming from the right).

In order to characterize these different domains in phase space, we introduce the coordinates

$$\xi \equiv \sqrt{\frac{m\omega}{2\hbar}}\left(x - \frac{p}{m\omega}\right) \tag{20}$$

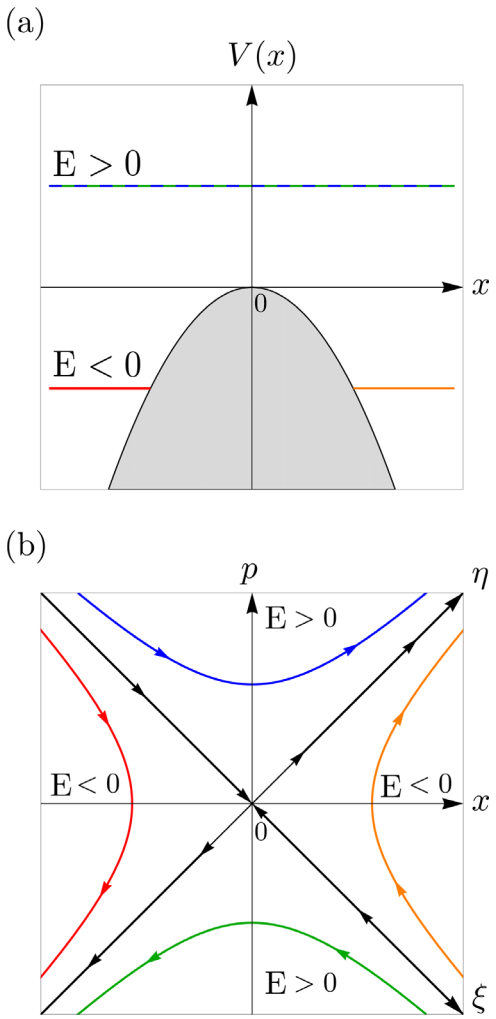

FIG. 1. The inverted harmonic oscillator illustrated in (a) position-energy and (b) phase space. For each energy E there exist two trajectories corresponding to an incoming particle from the left or right, respectively. (a) A classical particle with negative energy $E < 0$ (red and orange lines) is reflected at the potential barrier. On the contrary, a particle with positive energy $E > 0$ (blue and green lines) is able to surpass it. (b) The corresponding phase space trajectories $\{x_{\rm cl}(t), p_{\rm cl}(t)\}$, Eqs. (18) and (19), with the arrow indicating the direction of forward propagation in time t. Two distinct trajectories corresponding to the same energy E are separated by the two horizons $\xi = 0$ and $\eta = 0$, depicted along the diagonals, which divide phase space into four disjunct regions. On the half plane $\xi < 0$, the phase space trajectories (blue and red) describe the motion of a particle that approaches the potential barrier from the left, while for $\xi > 0$ the phase space trajectories (green and orange) correspond to an incoming particle from the right. In the domain $\xi\eta < 0$ the trajectories (blue and green) belong to a particle with positive energy $E > 0$, while in the domain $\xi\eta > 0$, the trajectories (red and orange) correspond to a particle with negative energy $E < 0$. A particle with energy $E = 0$ travels along the horizons $\xi = 0$ or $\eta = 0$, as indicated by the black arrows.

and

$$\eta \equiv \sqrt{\frac{m\omega}{2\hbar}}\left(x + \frac{p}{m\omega}\right), \tag{21}$$

where we have made use of the Planck constant $\hbar$ to arrive at dimensionless quantities. Consequently, with Eqs. (20) and (21), the Hamiltonian $H(x, p)$, Eq. (15), can be expressed in the form

$$H = -\frac{\hbar\omega}{2}(\xi\eta + \eta\xi), \tag{22}$$

which is invariant under the exchange of the coordinates ξ and η. Here, we have maintained the specific order in which these coordinates enter.

Next, we focus on the separatrices $\xi = 0$ and $\eta = 0$, depicted by the black diagonal lines in Fig. 1(b), which divide phase space into four disjunct regions. Analogous to an event horizon of a black hole that leads to a causal separation of different regions in spacetime, the lines $\xi = 0$ and $\eta = 0$ restrict the accessible regions in phase space. For this reason, we refer to them as *horizons* in *phase space*.

B. Origin of the logarithmic singularity

We are now in the position to reveal the intimate relation between the inverted harmonic oscillator and the logarithmic dependence that is characteristic for this system.

For this purpose, we recall the Hamilton equations of motion given by Eqs. (16) and (17). In the coordinates ξ and η, they read

$$\dot{\xi} = \frac{1}{\hbar}\frac{\partial H}{\partial \eta}, \tag{23}$$

$$\dot{\eta} = -\frac{1}{\hbar}\frac{\partial H}{\partial \xi}. \tag{24}$$

By inserting the Hamiltonian H, Eq. (22), of the inverted harmonic oscillator, Eqs. (23) and (24) reduce to the *logarithmic derivatives*

$$\frac{\dot{\xi}}{\xi} = -\omega, \tag{25}$$

$$\frac{\dot{\eta}}{\eta} = \omega. \tag{26}$$

As solution of Eqs. (25) and (26), the classical phase space trajectory in the coordinates ξ and η takes the simple form

$$\xi_{\mathrm{cl}}(t) = \xi_0 \exp(-\omega t), \tag{27}$$

$$\eta_{\mathrm{cl}}(t) = \eta_0 \exp(\omega t), \tag{28}$$

where the initial values ξ_0 and η_0 are assumed at time $t = 0$. We note that Eqs. (27) and (28) agree with the expressions for the classical phase space trajectories presented in Eqs. (18) and (19) with regard to position x and momentum p, as could be shown by using Eqs. (20) and (21).

In Fig. 2, we depict the phase space trajectories for particles with different initial conditions ξ_0 and η_0. In agreement with Eqs. (27) and (28), we observe that the motion of a classical particle in the inverted harmonic oscillator can be obtained by *dilations* of the phase space coordinates ξ and η. While the coordinate ξ_0 is scaled by $\exp(-\omega t)$, the coordinate η_0 experiences a scaling with regard to the reciprocal factor $\exp(\omega t)$ yielding the phase space coordinates of the particle at a later time t.

As a consequence, for any time t, each classical trajectory is restricted to a particular quadrant of phase space that is determined by

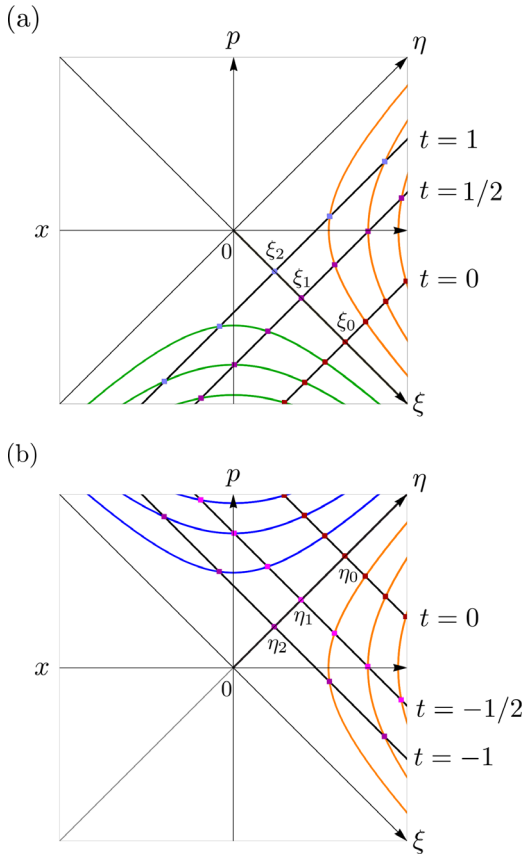

FIG. 2. Phase space trajectories demonstrating (a) the forward and (b) the backward propagation in time for a classical particle in the inverted harmonic oscillator. The horizons, depicted by the black diagonals, separate trajectories associated with negative energy $E < 0$ (orange) and positive energy $E > 0$ (green and blue). (a) The initial conditions are chosen such that all particles have the same value $\xi_0 > 0$ at time $t = 0$. At later times $t = 1/2$ and $t = 1$, these particles all share the same ξ-coordinate ξ_1 and ξ_2, respectively, as evident from Eq. (27). Accordingly, in the limit $t \to \infty$ all of them approach the horizon $\xi = 0$. (b) The initial conditions are chosen such that all particles have the same value $\eta_0 > 0$ at time $t = 0$. For earlier times $t = -1/2$ and $t = -1$ they share the same η-coordinate η_1 and η_2, respectively, as evident from Eq. (28). Accordingly, in the limit $t \to -\infty$ all of them approach the horizon $\eta = 0$.

the sign of the initial values ξ_0 and η_0. According to Eq. (22), these phase space trajectories are associated with the energy $E = -\hbar\omega\xi_0\eta_0$. Consequently, a particle located initially on the horizon $\xi_0 = 0$ or $\eta_0 = 0$ travels along the respective horizon with a vanishing energy $E = 0$.

First, we focus on particles that travel *forward* in time and share the same initial value $\xi_0 > 0$ at time $t = 0$, as displayed in Fig. 2(a). According to Eq. (25), it then takes the time

$$t = \frac{1}{\omega}\ln\left(\frac{\xi_0}{\xi_1}\right) \tag{29}$$

to reach the coordinate ξ_1. Consequently, at this time, *all particles* with initial coordinate ξ_0 reach the same ξ-coordinate ξ_1, as evident from

Fig. 1. Moreover, due to the *logarithmic dependence* in Eq. (29), these particles never reach the horizon $\xi = 0$ in a finite amount of time.[31]

Next, we turn to particles traveling *backwards* in time with an identical value $\eta_0 > 0$ at time $t = 0$, as depicted in Fig. 2(b). Here, it takes the time

$$t = -\frac{1}{\omega} \ln\left(\frac{\eta_0}{\eta_1}\right) \tag{30}$$

for *all particles* to reach the η-coordinate η_1 according to Eq. (28). Thus, the horizon $\eta = 0$ cannot be reached within a finite duration.

This behavior is a consequence of the fact that time reversal leads to a reflection of the momentum $p \to -p$ which, according to Eqs. (20) and (21), corresponds to the exchange $\xi \leftrightarrow \eta$ of the phase space coordinates ξ and η. Indeed, the reflection $p \to -p$ establishes the connection between the phase space trajectories displayed in Figs. 2(a) and 2(b).

In conclusion, we emphasize three important properties of the inverted harmonic oscillator: (i) the dynamics of a classical particle in the inverted harmonic oscillator can be obtained by *dilations* of the phase space coordinates ξ and η. Here, the scale factor is governed by the time t. For one of these phase space coordinates, the scale factor is the reciprocal of the other one. (ii) The *horizons* $\xi = 0$ and $\eta = 0$ separate different domains in phase space which distinguish overall aspects of a particular motion. In particular, these are the direction of the incoming particle, as expressed by the initial momentum $p < 0$ and $p > 0$, and the behavior at the potential barrier, as determined by the energy $E < 0$ and $E > 0$. Indeed, the horizons of an inverted harmonic oscillator, separating disjunct regions of phase space, remind of the event horizon of a black hole that cuts apart different domains of spacetime. (iii) The emergence of the *logarithmic singularity* in time, as presented in Eqs. (29) and (30), is a characteristic feature that occurs at the horizons in phase space of an inverted harmonic oscillator. Analogously, at the event horizon of a black hole, a logarithmic singularity also occurs in the mode functions of emitted Hawking radiation as shown in Sec. II.

IV. QUANTUM FEATURES OF THE INVERTED HARMONIC OSCILLATOR

In Sec. III, we have demonstrated that already a classical inverted harmonic oscillator points to several features that are familiar from Hawking radiation. The relationship between Hawking radiation and the inverted harmonic oscillator becomes even more evident when we turn to the quantum domain. Due the quadratic dependence of this particular potential, the classical and quantum dynamical equations of motion in the inverted harmonic oscillator are closely related to each other. However, the energy eigenstates as particular quantum states are the key to a deeper understanding of the logarithmic singularity.

In the following, we first introduce the relevant operators and quantum states that are required for our analysis. Next, we focus on the form of the energy eigenstates of the inverted harmonic oscillator, displaying a horizon in combination with a logarithmic phase singularity when represented in a suitable basis. As a consequence of the Fourier transform of a logarithmic phase, we then demonstrate the emergence of a functional dependence that resembles the Fermi–Dirac statistics.

As shown in Sec. II, a horizon, a logarithmic phase, and a Fourier transform of the mode function also play a crucial role in the context of Hawking radiation. Here, they lead to the appearance of a Bose–Einstein statistics. For this reason, these three ingredients establish a close relationship between the evaporation of a black hole and an inverted harmonic oscillator. However, in case of the inverted harmonic oscillator, the corresponding energy eigenstates do not display a horizon nor a logarithmic phase singularity in position representation. Indeed, only remnants of these features remain visible and appear, for instance, in the asymptotic expansion of the corresponding wave function. In the present section, we reveal these secrets of the energy eigenstates of the inverted harmonic oscillator.

A. Relevant operators and quantum states

We start our analysis by considering the Hamiltonian

$$\hat{H} = \frac{\hat{p}^2}{2m} - \frac{1}{2} m\omega^2 \hat{x}^2 \tag{31}$$

for a *quantum particle* of mass m subject to an inverted harmonic oscillator of steepness ω as resulting from Eq. (15). Here, the position $\hat{x}$ and the momentum operator $\hat{p}$ are subject to the familiar commutation relation

$$[\hat{x}, \hat{p}] = \mathrm{i}\hbar. \tag{32}$$

In order to reflect the phase space structure presented in Fig. 1(b), we introduce the operators[29,31]

$$\hat{\xi} \equiv \sqrt{\frac{m\omega}{2\hbar}}\left(\hat{x} - \frac{\hat{p}}{m\omega}\right) \tag{33}$$

and

$$\hat{\eta} \equiv \sqrt{\frac{m\omega}{2\hbar}}\left(\hat{x} + \frac{\hat{p}}{m\omega}\right) \tag{34}$$

in analogy to Eqs. (20) and (21).

Although $\hat{\xi}$ and $\hat{\eta}$ are Hermitian operators, their form reminds of the annihilation and creation operator of the harmonic oscillator as obtained up to an overall phase for an imaginary value of ω. Moreover, these operators satisfy the commutation relation

$$[\hat{\xi}, \hat{\eta}] = \mathrm{i}, \tag{35}$$

according to Eqs. (32)–(34). Thus, besides a rescaling, the operators $\hat{\xi}$ and $\hat{\eta}$ reflect a canonical transformation of the position $\hat{x}$ and the momentum operator $\hat{p}$.

Based on the Hermitian operators $\hat{\xi}$, Eq. (33), and $\hat{\eta}$, Eq. (34), we define the states $|\xi\rangle$ and $|\eta\rangle$ via the eigenvalue equations

$$\hat{\xi}|\xi\rangle = \xi|\xi\rangle \tag{36}$$

and

$$\hat{\eta}|\eta\rangle = \eta|\eta\rangle, \tag{37}$$

with the real-valued eigenvalues ξ and η, respectively.

Due to the commutation relation Eq. (35), the states $|\xi\rangle$ and $|\eta\rangle$ are related by the Fourier transform

$$\langle\xi|\eta\rangle = \frac{1}{\sqrt{2\pi}} \exp(\mathrm{i}\xi\eta). \tag{38}$$

These particular basis states define the representation that is used in our subsequent analysis.[43]

With the help of Eqs. (33)–(35), the Hamiltonian $\hat{H}$, Eq. (31), can then be cast into the form

$$\hat{H} = -\frac{\hbar\omega}{2}\left(\hat{\xi}\,\hat{\eta} + \hat{\eta}\,\hat{\xi}\right) \tag{39}$$

in agreement with Eq. (22). We point out the invariance of the Hamiltonian $\hat{H}$ under the exchange of the operators $\hat{\xi}$ and $\hat{\eta}$. Moreover, we note that $\hat{H}$ corresponds to the Hermitian form of the Berry–Keating Hamiltonian.[15]

Consequently, the energy eigenstates $|\varepsilon\rangle$ of the inverted harmonic oscillator are defined as solutions of the eigenvalue equation

$$\hat{H}|\varepsilon\rangle = \hbar\omega\varepsilon|\varepsilon\rangle \tag{40}$$

for the Hermitian Hamiltonian $\hat{H}$, Eq. (39), with real-valued dimensionless energy ε. We note that, more generally, eigenstates of the unbounded Hamiltonian $\hat{H}$ with complex eigenvalues can also be constructed.[44,45]

B. The energy eigenstates and the logarithmic phase singularity

We are now in the position to determine the energy eigenstates $|\varepsilon\rangle$ of the inverted harmonic oscillator by considering their projection onto the states $|\xi\rangle$, Eq. (36), and $|\eta\rangle$, Eq. (37). With the help of Eqs. (35) and (39), the eigenvalue equation (40) in ξ-representation takes the form

$$\xi\frac{\mathrm{d}}{\mathrm{d}\xi}\langle\xi|\varepsilon\rangle = \left(-\frac{1}{2} - \mathrm{i}\varepsilon\right)\langle\xi|\varepsilon\rangle. \tag{41}$$

Analogously, the eigenvalue equation (40) in η-representation reads

$$\eta\frac{\mathrm{d}}{\mathrm{d}\eta}\langle\eta|\varepsilon\rangle = \left(-\frac{1}{2} + \mathrm{i}\varepsilon\right)\langle\eta|\varepsilon\rangle. \tag{42}$$

We emphasize that the factor $-1/2$ in Eqs. (41) and (42) results from the *non-commutativity* of the operators $\hat{\xi}$ and $\hat{\eta}$, as presented in Eq. (35). In addition, due to the invariance of the Hamiltonian $\hat{H}$, Eq. (39), under the exchange $\hat{\xi} \leftrightarrow \hat{\eta}$, both the ξ- and η-representation lead to the almost identical form of the differential equations (41) and (42). However, they differ by the sign in front of the eigenvalue ε.

Furthermore, we point out the non-analytic behavior of $\langle\xi|\varepsilon\rangle$ at $\xi = 0$ due to the right-hand side of Eq. (41), and similarly of $\langle\eta|\varepsilon\rangle$ at $\eta = 0$ in Eq. (42). Indeed, this is due to a branch point that occurs at the horizons in phase space. As a consequence, there exist two linear independent solutions to each of these equations.

In agreement with Ref. 29, every energy eigenstate $|\varepsilon\rangle$ can then be expressed as a linear combination

$$|\varepsilon\rangle = \alpha_+(\varepsilon)|\Psi_\varepsilon^+\rangle + \alpha_-(\varepsilon)|\Psi_\varepsilon^-\rangle \tag{43}$$

of two orthogonal energy eigenstates $|\Psi_\varepsilon^\pm\rangle$ with coefficients $\alpha_\pm(\varepsilon)$. We define these particular states by their ξ-representation $\Psi_\varepsilon^\pm(\xi) \equiv \langle\xi|\Psi_\varepsilon^\pm\rangle$, where

$$\Psi_\varepsilon^\pm(\xi) = \frac{1}{\sqrt{2\pi|\xi|}}\exp\left(-\mathrm{i}\varepsilon\ln|\xi|\right)\Theta(\pm\xi) \tag{44}$$

is a solution of Eq. (41). Here, we have introduced the Heaviside step function

$$\Theta(x) \equiv \begin{cases} 1, & x \geq 0, \\ 0, & x < 0. \end{cases} \tag{45}$$

The particular set of eigenstates $|\Psi_\varepsilon^\pm\rangle$ of the Hamiltonian $\hat{H}$, Eq. (39), with energy ε is characterized by the fact that the ξ-representation $\Psi_\varepsilon^\pm(\xi)$, Eq. (44), vanishes for $(+)$ negative and $(-)$ positive values of ξ, as demonstrated in Fig. 3. There we depict in red the real and imaginary part of the two orthogonal energy eigenstates (a) $\Psi_\varepsilon^+(\xi)$ and (b) $\Psi_\varepsilon^-(\xi)$ of the inverted harmonic oscillator as a function of the coordinate ξ.

We clearly observe the horizon at $\xi = 0$ which separates the non-vanishing part of the wave function from the zero solution. When approaching the horizon $\xi = 0$ from the direction $\xi > 0$ $(+)$ and $\xi < 0$ $(-)$, both the *amplitude* and the *phase* of $\Psi_\varepsilon^\pm(\xi)$ diverge and result in an increasing radius, presented by the orange envelope, and a faster winding of the spiral. In addition, we point out that the dimensionless energy ε only enters as magnitude of the logarithmic phase $-\varepsilon\ln|\xi|$ of the energy eigenfunctions $\Psi_\varepsilon^\pm(\xi)$, while the amplitude is independent of ε.

Alternatively, every energy eigenstate $|\varepsilon\rangle$ can be expressed as a superposition

$$|\varepsilon\rangle = \beta_+(\varepsilon)|\Phi_\varepsilon^+\rangle + \beta_-(\varepsilon)|\Phi_\varepsilon^-\rangle \tag{46}$$

of the two orthogonal energy eigenstates $|\Phi_\varepsilon^\pm\rangle$ with coefficients $\beta_\pm(\varepsilon)$. We define these states by their η-representation $\Phi_\varepsilon^\pm(\eta) \equiv \langle\eta|\Phi_\varepsilon^\pm\rangle$, where

$$\Phi_\varepsilon^\pm(\eta) = \frac{1}{\sqrt{2\pi|\eta|}}\exp\left(\mathrm{i}\varepsilon\ln|\eta|\right)\Theta(\pm\eta) \tag{47}$$

is a solution of Eq. (42) with the Heaviside step function Θ as defined by Eq. (45). Consequently, the eigenstates $|\Phi_\varepsilon^\pm\rangle$ are characterized by the fact that their η-representation vanishes for negative or positive values of η, as facilitated by the non-analytic behavior at $\eta = 0$ in Eq. (42).

Each set of energy eigenstates forms a complete basis with the completeness relations

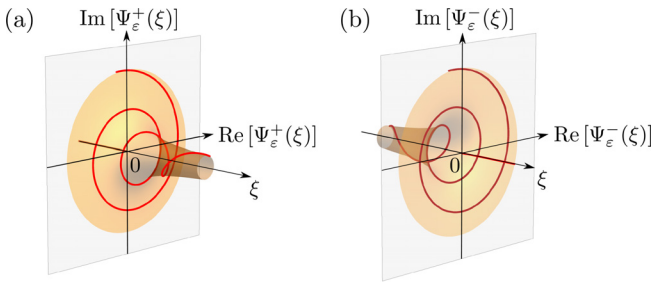

FIG. 3. Energy eigenfunctions $\Psi_\varepsilon^\pm(\xi)$, Eq. (44), of the inverted harmonic oscillator for the dimensionless energy $\varepsilon = 5$. The wave functions (a) $\Psi_\varepsilon^+(\xi)$ and (b) $\Psi_\varepsilon^-(\xi)$ vanish for $\xi < 0$ and $\xi > 0$, respectively. When approaching the horizon $\xi = 0$ from the opposite direction, the amplitude of the wave function increases independently of ε, as shown by the orange envelope and the enlarged radius of the spiral. The logarithmic dependence of the phase on ξ instead results in a faster winding close to the horizon as governed by the dimensionless energy ε.

$$\mathbb{1} = \int_{-\infty}^{\infty} \mathrm{d}\varepsilon \left(|\Psi_\varepsilon^+\rangle\langle\Psi_\varepsilon^+| + |\Psi_\varepsilon^-\rangle\langle\Psi_\varepsilon^-| \right) \tag{48}$$

and

$$\mathbb{1} = \int_{-\infty}^{\infty} \mathrm{d}\varepsilon \left(|\Phi_\varepsilon^+\rangle\langle\Phi_\varepsilon^+| + |\Phi_\varepsilon^-\rangle\langle\Phi_\varepsilon^-| \right), \tag{49}$$

where $\mathbb{1}$ denotes the identity.

Moreover, as evident from Eqs. (44) and (47), the energy eigenstates are normalized according to the conditions

$$\int_{-\infty}^{\infty} \mathrm{d}\xi \left[\Psi_\varepsilon^s(\xi)\right]^* \Psi_{\varepsilon'}^{s'}(\xi) = \delta_{s,s'}\delta(\varepsilon - \varepsilon') \tag{50}$$

and

$$\int_{-\infty}^{\infty} \mathrm{d}\eta \left[\Phi_\varepsilon^s(\eta)\right]^* \Phi_{\varepsilon'}^{s'}(\eta) = \delta_{s,s'}\delta(\varepsilon - \varepsilon'), \tag{51}$$

with the indices $s, s' = \pm$ labeling the two degenerate solutions. Here, $\delta_{s,s'}$ denotes the Kronecker delta and $\delta(\varepsilon - \varepsilon')$ is the Dirac delta function. In this regard, the functions $\Psi_\varepsilon^\pm(\xi)$ and $\Phi_\varepsilon^\pm(\eta)$ are not square-integrable.

Despite the seemingly similar form of the solutions $\Psi_\varepsilon^\pm(\xi)$, Eq. (44), and $\Phi_\varepsilon^\pm(\eta)$, Eq. (47), we emphasize that each of them corresponds to a different eigenstate $|\Psi_\varepsilon^\pm\rangle$ and $|\Phi_\varepsilon^\pm\rangle$ of the Hamiltonian $\hat{H}$, Eq. (39), with dimensionless energy ε.

In summary, the inverted harmonic oscillator displays the following characteristic features: (i) it has a continuous spectrum and a two-fold degeneracy with regard to the energy ε, as expressed by the orthogonal solutions $\Psi_\varepsilon^\pm(\xi)$, Eq. (44), or $\Phi_\varepsilon^\pm(\eta)$, Eq. (47), respectively. (ii) As a consequence of the Heaviside step function defined by Eq. (45), the solutions $\Psi_\varepsilon^\pm(\xi)$ and $\Phi_\varepsilon^\pm(\eta)$ only possess non-vanishing contributions in a *half-plane* of phase space with regard to the ξ- and η-domain, respectively. This feature is reminiscent of the *event horizon* of a black hole in *spacetime*. However, here two *horizons* emerge in *phase space*. (iii) For $\varepsilon \neq 0$, the energy eigenstates display both a *phase singularity* and an *amplitude singularity* at the horizons $\xi = 0$ and $\eta = 0$, respectively. While the logarithmic phase singularity is reminiscent of the logarithmic singularity in the mode function of a quantized bosonic field at the event horizon of a black hole,[5] an additional amplitude singularity induced by the reciprocal square-root dependency arises in the system of the inverted harmonic oscillator.

C. The Fourier transform and the Fermi–Dirac statistics

In the context of a black hole, it is the Fourier transform of a mode function with a logarithmic phase singularity that determines the number of particles emitted by Hawking radiation in this mode.[5] For a massless scalar field of integer spin, this number follows a Bose–Einstein statistics that is governed by the ratio of the frequency of the wave and the surface gravity of the black hole as presented in Sec. II. We now demonstrate that a related feature is present in the simple model of an inverted harmonic oscillator. Also, here, a Fourier transform of a logarithmic phase singularity is of crucial relevance.

In order to illustrate this fact, we consider the η-representation

$$\langle\eta|\Psi_\varepsilon^+\rangle = \int_{-\infty}^{\infty} \mathrm{d}\xi \, \langle\eta|\xi\rangle\langle\xi|\Psi_\varepsilon^+\rangle \tag{52}$$

of the energy eigenstate $|\Psi_\varepsilon^+\rangle$, where we have inserted the identity with regard to the basis states $|\xi\rangle$ for $\xi \in \mathbb{R}$, Eq. (36), on the right-hand side.

By making use of Eq. (38), we express Eq. (52) as the Fourier transform

$$\langle\eta|\Psi_\varepsilon^+\rangle = \frac{1}{2\pi}\int_0^{\infty} \mathrm{d}\xi \, \frac{\exp\left(-\mathrm{i}\varepsilon\ln|\xi|\right)}{\sqrt{\xi}} \exp\left(-\mathrm{i}\xi\eta\right) \tag{53}$$

of the energy eigenfunction $\Psi_\varepsilon^+(\xi)$, Eq. (44), displaying a logarithmic phase singularity at $\xi \to 0+$ in combination with an amplitude singularity induced by the reciprocal square root.

Due to the particular form of the energy eigenfunction $\Psi_\varepsilon^+(\xi)$, Eq. (53) corresponds not only to the *Fourier transform* of $|\xi|^{-1/2-\mathrm{i}\varepsilon}\Theta(\xi)$ but also to the *Mellin transform* of the plane wave $\exp(-\mathrm{i}\xi\eta)$. As such, Eq. (53) indeed constitutes an example of the quantum Mellin transform.[46] In addition, we point out that it also represents a fractional Weyl integral.[47] This interesting link between the inverted harmonic oscillator with its horizons in phase space and the field of *fractional calculus* requires further exploration.

Next, we evaluate the integral in Eq. (53) and arrive at the expression

$$\langle\eta|\Psi_\varepsilon^+\rangle = \frac{\Gamma\left(\frac{1}{2} - \mathrm{i}\varepsilon\right)}{\sqrt{2\pi}} \left[\mathrm{e}^{-\frac{\mathrm{i}\pi}{4} - \frac{\pi\varepsilon}{2}} \Phi_\varepsilon^+(\eta) + \mathrm{e}^{\frac{\mathrm{i}\pi}{4} + \frac{\pi\varepsilon}{2}} \Phi_\varepsilon^-(\eta) \right], \tag{54}$$

where Γ denotes the gamma function. Accordingly, the state

$$|\Psi_\varepsilon^+\rangle = S_+(\varepsilon)|\Phi_\varepsilon^+\rangle + S_-(\varepsilon)|\Phi_\varepsilon^-\rangle \tag{55}$$

can be expressed as a superposition of the energy eigenstates $|\Phi_\varepsilon^\pm\rangle$, whose η-representation is given by Eq. (47), where we have introduced the coefficients

$$S_\pm(\varepsilon) \equiv \frac{\Gamma\left(\frac{1}{2} - \mathrm{i}\varepsilon\right)}{\sqrt{2\pi}} \exp\left[\mp \left(\frac{\mathrm{i}\pi}{4} + \frac{\pi\varepsilon}{2} \right) \right]. \tag{56}$$

Analogously, we obtain the decomposition

$$|\Psi_\varepsilon^-\rangle = S_-(\varepsilon)|\Phi_\varepsilon^+\rangle + S_+(\varepsilon)|\Phi_\varepsilon^-\rangle \tag{57}$$

for the energy eigenstate $|\Psi_\varepsilon^-\rangle$, whose ξ-representation is given by Eq. (44).

The coefficients $S_\pm(\varepsilon)$, Eq. (56), constitute the elements of the unitary scattering matrix

$$\mathbf{S}(\varepsilon) \equiv \begin{pmatrix} S_+(\varepsilon) & S_-(\varepsilon) \\ S_-(\varepsilon) & S_+(\varepsilon) \end{pmatrix}, \tag{58}$$

which establishes the relation

$$\boldsymbol{\beta}(\varepsilon) = \mathbf{S}(\varepsilon)\boldsymbol{\alpha}(\varepsilon) \tag{59}$$

for the vectors $\boldsymbol{\alpha}(\varepsilon) \equiv [\alpha_+(\varepsilon), \alpha_-(\varepsilon)]^{\mathrm{T}}$ and $\boldsymbol{\beta}(\varepsilon) \equiv [\beta_+(\varepsilon), \beta_-(\varepsilon)]^{\mathrm{T}}$ in Eqs. (43) and (46), as evident from Eqs. (55) and (57). We point out that the S-matrix $\mathbf{S}(\varepsilon)$, Eq. (58), has already been related to scattering off a black hole.[27,34]

Next, we turn to the probability density

$$|\langle\eta|\Psi_\varepsilon^+\rangle|^2 = |S_+(\varepsilon)|^2|\langle\eta|\Phi_\varepsilon^+\rangle|^2 + |S_-(\varepsilon)|^2|\langle\eta|\Phi_\varepsilon^-\rangle|^2 \tag{60}$$

in η-representation by making use of the orthogonality of the states $|\Phi_\varepsilon^\pm\rangle$, Eq. (51).

By applying the relation

$$\Gamma\left(\frac{1}{2}-\mathrm{i}\varepsilon\right)\Gamma\left(\frac{1}{2}+\mathrm{i}\varepsilon\right)=\frac{\pi}{\cosh(\pi\varepsilon)} \tag{61}$$

for the gamma function, we identify the weights

$$|S_\pm(\varepsilon)|^2=\frac{1}{1+\mathrm{e}^{\pm 2\pi\varepsilon}} \tag{62}$$

being displayed in Fig. 4.

Finally, we make use of Eqs. (47) and (62) in order to recast Eq. (60) in the form

$$|\langle\eta|\Psi_\varepsilon^+\rangle|^2=\frac{1}{2\pi|\eta|}\left[\frac{\Theta(\eta)}{1+\mathrm{e}^{2\pi\varepsilon}}+\frac{\Theta(-\eta)}{1+\mathrm{e}^{-2\pi\varepsilon}}\right], \tag{63}$$

determining the absolute value squared for the overlap of the state $|\eta\rangle$ and the energy eigenstate $|\Psi_\varepsilon^+\rangle$.

It is a fascinating coincidence that the weights $|S_\pm(\varepsilon)|^2$, Eq. (62), actually resemble the *Fermi–Dirac distribution*[48] as governed by the dimensionless energy $\pm\varepsilon$. In contrast to thermodynamics where the characteristic energy of the system is given by the product $k_\mathrm{B}T$ of the Boltzmann constant k_B and the temperature T, it is the product $\hbar\omega$ of the Planck constant $\hbar$ and the steepness ω divided by $4\pi^2$, which defines the energy scale of the inverted harmonic oscillator as evident from Eqs. (40) and (63).

We now summarize the main properties of the weights $|S_\pm(\varepsilon)|^2$ as defined by Eq. (62). First, we identify the relation

$$|S_+(\varepsilon)|^2+|S_-(\varepsilon)|^2=1, \tag{64}$$

which is valid for any value of ε, as evident from Fig. 4, and expected for the two coefficients in the decomposition of the state $|\Psi_\varepsilon^+\rangle$, Eq. (55), due to normalization.

Second, in the classical case of the inverted harmonic oscillator, the particles move along the horizons in phase space for a vanishing energy $E=0$ as shown in Fig. 1. In the quantum mechanical case, it is instead the vanishing energy $\varepsilon=0$ of the energy eigenstate $|\Psi_\varepsilon^+\rangle$ that leads to equal weights $|S_+(0)|^2=|S_-(0)|^2=1/2$.

Third, as depicted in Fig. 4, we obtain the weights $|S_\pm(\varepsilon)|^2\to 1$ for the energy $\varepsilon\to\mp\infty$, respectively. Accordingly, for $\varepsilon\to\infty$, the main contribution to the state $|\Psi_\varepsilon^+\rangle$ originates from the state $|\Phi_\varepsilon^-\rangle$. At first, this seems to be a counter-intuitive result. Indeed, for any value of ε, there are different horizons in phase space associated with the states $|\Psi_\varepsilon^+\rangle$ and $|\Phi_\varepsilon^-\rangle$, as shown by Eqs. (44) and (47), respectively. We will resolve this issue in Sec. V.

Finally, we point out that the probabilities $|S_\pm(\varepsilon)|^2$ in Eq. (62) define the transmission $T(\varepsilon)\equiv|S_-(\varepsilon)|^2$ and reflection coefficient $R(\varepsilon)\equiv|S_+(\varepsilon)|^2$ of the inverted harmonic oscillator,[30,31,36,41] in agreement with the scattering matrix given by Eq. (58). Consequently, the state $|\Phi_\varepsilon^-\rangle$ corresponds to the transmitted part of $|\Psi_\varepsilon^+\rangle$, while $|\Phi_\varepsilon^+\rangle$ describes the reflected one. The higher the energy eigenvalue ε of the eigenstate state $|\Psi_\varepsilon^+\rangle$, the higher the probability $T(\varepsilon)$ of the quantum particle to be transmitted. At the same time, the probability $R(\varepsilon)$ of reflection decreases.

In summary, analog to the number of particles for Hawking radiation emitted by black holes, the transmission and reflection coefficient of the inverted harmonic oscillator resemble a particular quantum statistics. This feature is a consequence of the Fourier transform of a logarithmic phase singularity that is contained in the function $\Psi_\varepsilon^\pm(\xi)$, Eq. (44). However, the additional amplitude singularity, induced by the reciprocal square root, leads to the emergence of the Fermi–Dirac instead of the Bose–Einstein statistics.[5,13]

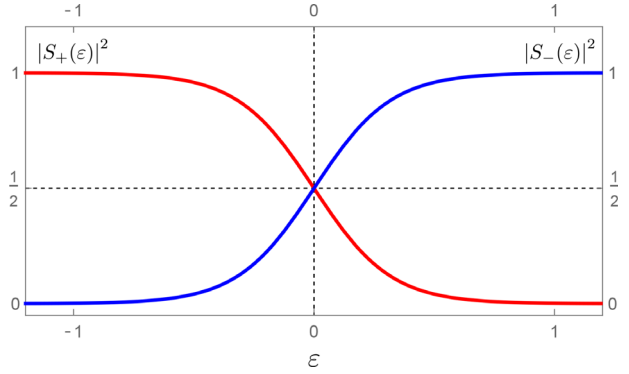

FIG. 4. The transmission $|S_-(\varepsilon)|^2$ and reflection coefficient $|S_+(\varepsilon)|^2$ of the inverted harmonic oscillator resemble a Fermi–Dirac distribution, shown as a function of the dimensionless energy ε. We depict the probabilities $|S_+(\varepsilon)|^2$ (red) and $|S_-(\varepsilon)|^2$ (blue), Eq. (62), which according to Eq. (55) describe the respective contribution of the states $|\Phi_\varepsilon^+\rangle$ and $|\Phi_\varepsilon^-\rangle$ to the energy eigenstate $|\Psi_\varepsilon^+\rangle$. The higher the energy ε of the state $|\Psi_\varepsilon^+\rangle$, the higher is the probability $|S_-(\varepsilon)|^2$ and the lower is $|S_+(\varepsilon)|^2$.

D. The horizons and singularities are hidden in position representation

In Secs. IV B and IV C, we have uncovered the horizons and the logarithmic phase singularity intrinsic to the inverted harmonic oscillator by analyzing the states $|\Psi_\varepsilon^\pm\rangle$ and $|\Phi_\varepsilon^\pm\rangle$ in ξ- and η-representation, respectively. We have presented the appearance of a functional dependence that resembles the Fermi–Dirac statistics which connects these two representations of the energy eigenstates. However, as demonstrated in the following, these interesting features familiar from the context of Hawking radiation remain hidden in position representation.

For this purpose, we consider the position representation $\psi_\varepsilon^\pm(x)\equiv\langle x|\Psi_\varepsilon^\pm\rangle$ and $\phi_\varepsilon^\pm(x)\equiv\langle x|\Phi_\varepsilon^\pm\rangle$ of the energy eigenstates $|\Psi_\varepsilon^\pm\rangle$, Eq. (44), and $|\Phi_\varepsilon^\pm\rangle$, Eq. (47). Here, $|x\rangle$ denotes the eigenstate of the position operator $\hat{x}$ with eigenvalue x.

As derived in Appendix B, these wave functions take the form

$$\psi_\varepsilon^\pm(x)=\mathscr{N}_-(\varepsilon)D_{-\frac{1}{2}+\mathrm{i}\varepsilon}\left(\pm\mathrm{e}^{\mathrm{i}3\pi/4}\sqrt{\frac{2m\omega}{\hbar}}x\right) \tag{65}$$

and

$$\phi_\varepsilon^\pm(x)=\mathscr{N}_+(\varepsilon)D_{-\frac{1}{2}-\mathrm{i}\varepsilon}\left(\pm\mathrm{e}^{-\mathrm{i}3\pi/4}\sqrt{\frac{2m\omega}{\hbar}}x\right). \tag{66}$$

Here, $D_{-1/2\pm\mathrm{i}\varepsilon}$ denotes the parabolic cylinder function[49] and the normalization constant

$$\mathscr{N}_\pm(\varepsilon)\equiv\frac{\Gamma\left(\frac{1}{2}\pm\mathrm{i}\varepsilon\right)}{\sqrt{2\pi}}\left(\frac{m\omega}{2\hbar}\right)^{1/4}\mathrm{e}^{\varepsilon\pi/4} \tag{67}$$

is determined by the gamma function Γ. The functions $\psi_\varepsilon^\pm(x)$ and $\phi_\varepsilon^\pm(x)$ correspond to well-known solutions[31,33] of the Schrödinger equation for the inverted harmonic oscillator, as expressed in position representation in terms of the parabolic cylinder functions.

First, as evident from Eq. (65), the wave functions $\psi_\varepsilon^+(x)$ and $\psi_\varepsilon^-(x)$ are related to each other by a reflection $x \to -x$ in position. The same holds for $\phi_\varepsilon^+(x)$ and $\phi_\varepsilon^-(x)$ according to Eq. (66). Second, we note that the function $\phi_\varepsilon^\pm(x)$ is the complex conjugate of $\psi_\varepsilon^\pm(x)$. Apparently, the Hamiltonian $\hat{H}$, Eq. (31), remains invariant under the corresponding transformations of the operators $\hat{x}$ and $\hat{p}$.

In Fig. 5, we depict the energy eigenfunctions (a) $\psi_\varepsilon^+(x)$ and (b) $\psi_\varepsilon^-(x)$ of the inverted harmonic oscillator in combination with the corresponding probability density $|\psi_\varepsilon^\pm(x)|^2$. We clearly observe the relation $\psi_\varepsilon^-(x) = \psi_\varepsilon^+(-x)$ according to Eq. (65). As apparent from the probability density $|\psi_\varepsilon^\pm(x)|^2$, the wave function $\psi_\varepsilon^\pm(x)$ is associated with an incoming particle approaching the parabolic barrier from (a) right and (b) left. The oscillations in the domains (a) $x>0$ and (b) $x<0$ are caused by the interference of the incoming wave with the one reflected at the potential barrier. On the other hand, for (a) $x<0$ and (b) $x>0$ one identifies a decaying amplitude. Indeed, for negative energies $\varepsilon<0$, a non-vanishing probability in this domain is caused by tunneling[30,32] through, and for positive energies $\varepsilon>0$ by transmission beyond the parabolic barrier.

Furthermore, we notice from Fig. 5 that the wave function $\psi_\varepsilon^\pm(x)$ neither displays an amplitude singularity nor a phase singularity as one might have expected from the ξ-representation of the state $|\Psi_\varepsilon^\pm\rangle$ given by Eq. (44). In addition, the horizon is hidden at which these singularities would occur.

In order to demonstrate that traces of these features are still present in position representation, we consider the asymptotic behavior of the wave function $\psi_\varepsilon^+(x)$, Eq. (65). By applying the asymptotic

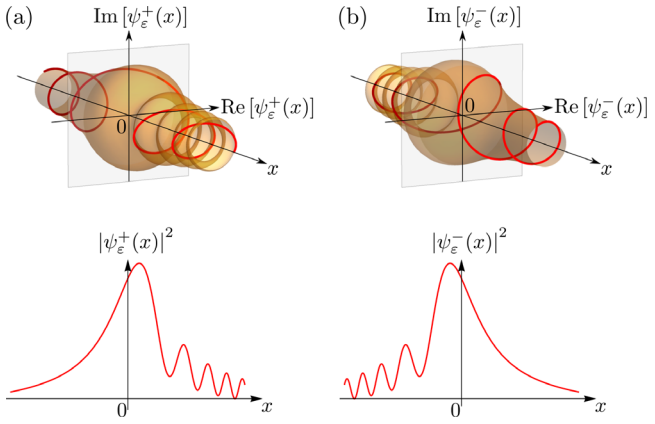

Fig. 5. Position representation of the energy eigenfunctions (a) $\psi_\varepsilon^+(x)$ and (b) $\psi_\varepsilon^-(x)$, Eq. (65), of the inverted harmonic oscillator for the dimensionless energy $\varepsilon = 1/2$. On the top, we depict real and imaginary parts of these functions in red, and on the bottom we present the corresponding probability density. Here, $\psi_\varepsilon^+(x)$ corresponds to an incoming particle from the right which is reflected at the barrier of the inverted harmonic oscillator and interfering with the incoming wave. Analogously, the wave function $\psi_\varepsilon^-(x)$ corresponds to a particle approaching the parabolic barrier from the left. In this regard, we notice the symmetry relation $|\psi_\varepsilon^+(x)|^2 = |\psi_\varepsilon^-(-x)|^2$ according to Eq. (65). In contrast to the ξ-representation of the states $|\Psi_\varepsilon^\pm\rangle$, depicted in Fig. 3, the horizon and the singularities remain hidden.

expansion[49] for the parabolic cylinder function $D_{-1/2\pm i\varepsilon}$, we obtain for $x \gg 1$ the expression

$$\psi_\varepsilon^+(x) \simeq \mathcal{N}_-(\varepsilon)\left[\mathrm{e}^{-\frac{3\pi\varepsilon}{4}+\mathrm{i}\left(\frac{m\omega}{2\hbar}x^2-\frac{3\pi}{8}\right)}\left|\sqrt{\frac{2m\omega}{\hbar}}x\right|^{-1/2+\mathrm{i}\varepsilon} + \frac{\sqrt{2\pi}}{\Gamma\left(\frac{1}{2}-\mathrm{i}\varepsilon\right)}\mathrm{e}^{-\frac{\pi\varepsilon}{4}-\mathrm{i}\left(\frac{m\omega}{2\hbar}x^2-\frac{\pi}{8}\right)}\left|\sqrt{\frac{2m\omega}{\hbar}}x\right|^{-1/2-\mathrm{i}\varepsilon}\right], \tag{68}$$

and for $x \ll -1$, we arrive at

$$\psi_\varepsilon^+(x) \simeq \mathcal{N}_-(\varepsilon)\mathrm{e}^{\frac{\pi\varepsilon}{4}+\mathrm{i}\left(\frac{m\omega}{2\hbar}x^2+\frac{\pi}{8}\right)}\left|\sqrt{\frac{2m\omega}{\hbar}}x\right|^{-1/2+\mathrm{i}\varepsilon}. \tag{69}$$

While the asymptotic expansion in Eq. (68) for $x \gg 1$ is composed of two terms, the one in Eq. (69) for $x \ll -1$ only consists of a single term. In Sec. V, we present an illustrative explanation for this manifestation of *Stokes phenomenon*.

Accordingly, Eqs. (68) and (69) both contain at least one of the terms $|x|^{-1/2\pm i\varepsilon}$ which are reminiscent of an amplitude and a logarithmic phase singularity at $x=0$. However, these asymptotic expansions are not applicable in the domain $|x|<1$. For this reason, these features remain hidden as evident from Fig. 5. Moreover, due to the slow decrease in the amplitude proportional to $1/\sqrt{|x|}$ for $|x| \ll 1$, the energy eigenstates of the inverted harmonic oscillator remain non-normalizable in position space.

In addition, it is interesting to note that the asymptotic expansions in Eqs. (68) and (69) contain a phase that is governed by a *quadratic* dependence on the position x. This is a characteristic feature of a wave that displays a focus after a certain time of free propagation.

V. PHASE SPACE ANALYSIS OF THE INVERTED HARMONIC OSCILLATOR

So far, we have explored the inverted harmonic oscillator in terms of the wave and matrix mechanics formulations of quantum mechanics. In particular, we have studied the emergence of horizons, the logarithmic phase singularity, and the intimidate relation to the Fermi–Dirac statistics. Moreover, we have shown that these features are only apparent in particular representations.

The physics of all these phenomena stands out most clearly when viewed in Wigner phase space,[50,51] which provides an intuitive illustration of quantum mechanics. Indeed, a quasi-probability distribution as the Wigner function does not rely on a particular representation. Instead, it depends on *two* phase space variables, such as position x and momentum p, or equivalently, the coordinates ξ and η. The Wigner function also builds a bridge between classical statistical mechanics and quantum mechanics in phase space. This intimidate relationship allows us to relate the results of Sec. III, obtained in classical phase space, with our subsequent study in the quantum domain.

In the following, we extend the analysis of the inverted harmonic oscillator in phase space as pursued in Refs. 29 and 30. The focus of these works lays on tunneling phenomena with regard to the parabolic barrier. In contrast, our interest rests on the horizons in phase space in combination with the emergence of a singularity, which relates to Hawking radiation emerging at the event horizon of a black hole.

For this purpose, we analyze different characteristic features that are intrinsic to the phase space representation of the energy eigenstates of the inverted harmonic oscillator.

First, we derive the Wigner functions of the energy eigenstates of the inverted harmonic oscillator based on their ξ- and η-representation. Next, we turn to an illustration of the properties of these particular states and relate their shape to the classical phase space trajectories. Subsequently, we review their dependence on the dimensionless energy with regard to the reflection and transmission at a parabolic barrier. We then focus on the horizons in phase space and reveal their relation to the occurrence of singularities in the inverted harmonic oscillator. Moreover, with the help of particular phase space projections, we reveal the emergence of a distribution that resembles the Fermi–Dirac statistics. Finally, we analyze why these features remain hidden in the position representation of quantum mechanics.

A. The Wigner functions of the energy eigenstates

In the following, we determine the Wigner functions for the energy eigenstates $|\Psi_\varepsilon^\pm\rangle$ and $|\Phi_\varepsilon^\pm\rangle$ of the inverted harmonic oscillator with dimensionless energy ε, as introduced in Sec. IV.

First, we focus on the Wigner function[50,51]

$$W_{\Psi,\varepsilon}^\pm(\xi,\eta)=\frac{1}{2\pi}\int_{-\infty}^{\infty}\mathrm{d}y\,\mathrm{e}^{-\mathrm{i}\eta y}\left\langle\Psi_\varepsilon^\pm|\xi-\frac{y}{2}\right\rangle\left\langle\xi+\frac{y}{2}\middle|\Psi_\varepsilon^\pm\right\rangle \tag{70}$$

corresponding to the energy eigenstate $|\Psi_\varepsilon^\pm\rangle$. Here, we have made use of the fact that, up to a rescaling, the coordinates ξ and η, defined by Eqs. (20) and (21), result from a canonical transformation of the phase space variables x and p under which the Wigner function transforms as a scalar.[29]

By inserting the wave function $\Psi_\varepsilon^\pm(\xi)=\langle\xi|\Psi_\varepsilon^\pm\rangle$, Eq. (44), in ξ-representation, we recast Eq. (70) as

$$W_{\Psi,\varepsilon}^\pm(\xi,\eta)=\frac{\Theta(\pm\xi)}{4\pi^2}\int_{\mp2\xi}^{\pm2\xi}\mathrm{d}y\,\frac{\exp\left(-\mathrm{i}\varepsilon\ln\left|\frac{\xi+\frac{y}{2}}{\xi-\frac{y}{2}}\right|\right)}{\sqrt{|\xi^2-\frac{y^2}{4}|}}\mathrm{e}^{-\mathrm{i}\eta y}, \tag{71}$$

where we have applied the relation

$$\Theta\left[\pm\left(\xi+\frac{y}{2}\right)\right]\Theta\left[\pm\left(\xi-\frac{y}{2}\right)\right]=\begin{cases}1, & \mp2\xi\le y\le\pm2\xi,\\ 0, & \text{else},\end{cases} \tag{72}$$

for the Heaviside step function defined by Eq. (45). With the help of the substitution $y'=\pm y/\xi$ in Eq. (71) we then arrive at the Wigner function

$$W_{\Psi,\varepsilon}^\pm(\xi,\eta)=\frac{1}{2\pi}w_\varepsilon(-\hbar\omega\xi\eta)\Theta(\pm\xi). \tag{73}$$

Here, we have introduced the weight function

$$w_\varepsilon(E)\equiv\frac{1}{\pi}\int_{-2}^{2}\mathrm{d}y'\,\frac{\exp\left(-\mathrm{i}\varepsilon\ln\left|\frac{2+y'}{2-y'}\right|\right)}{\sqrt{4-y'^2}}\mathrm{e}^{\mathrm{i}\frac{E}{\hbar\omega}y'}, \tag{74}$$

yielding the contribution to the Wigner function $W_{\Psi,\varepsilon}^\pm(\xi,\eta)$, Eq. (73), with regard to the classical energy $E=-\hbar\omega\xi\eta$ as given by Eq. (22). With the help of Eq. (61) the weight function can also be expressed as

$$w_\varepsilon(E)=\frac{\exp\left(-\mathrm{i}\frac{2E}{\hbar\omega}\right)}{\cosh(\pi\varepsilon)}\,{}_1\mathscr{F}_1\left(\frac{1}{2}-\mathrm{i}\varepsilon;1;\frac{4E}{\hbar\omega}\mathrm{i}\right) \tag{75}$$

in terms of the Kummer function of the first kind[49]

$${}_1\mathscr{F}_1(a;b;z)\equiv\frac{\Gamma(b)}{\Gamma(b-a)\Gamma(a)}\int_0^1\mathrm{d}t\,\mathrm{e}^{zt}t^{a-1}(1-t)^{b-a-1}. \tag{76}$$

Interestingly, similar to the wave function $\Psi_\varepsilon^+(\xi)$, Eq. (44), the weight function $w_\varepsilon(E)$, Eq. (74), also displays a logarithmic phase. However, this phase appears now within an integral and becomes singular at the boundaries of the integration region. Moreover, the phase singularity occurs in combination with an amplitude singularity as resulting from a reciprocal square root. Moreover, we note that, up to the normalization constant $1/(2\pi)$, the Wigner function $W_{\Psi,\varepsilon}^\pm(\xi,\eta)$, Eq. (73), coincides with the one derived in Ref. 30 as solution of the Moyal equations.

Next, we turn to the Wigner function

$$W_{\Phi,\varepsilon}^\pm(\xi,\eta)=\frac{1}{2\pi}\int_{-\infty}^{\infty}\mathrm{d}q\,\mathrm{e}^{\mathrm{i}\xi q}\left\langle\Phi_\varepsilon^\pm|\eta-\frac{q}{2}\right\rangle\left\langle\eta+\frac{q}{2}\middle|\Phi_\varepsilon^\pm\right\rangle \tag{77}$$

corresponding to the energy eigenstate $|\Phi_\varepsilon^\pm\rangle$. With the help of the η-representation $\Phi_\varepsilon^\pm(\eta)=\langle\eta|\Phi_\varepsilon^\pm\rangle$, Eq. (47), we recast Eq. (77) as

$$W_{\Phi,\varepsilon}^\pm(\xi,\eta)=\frac{1}{2\pi}w_\varepsilon(-\hbar\omega\xi\eta)\Theta(\pm\eta) \tag{78}$$

in terms of the weight function w_ε, Eq. (74), in an analogous way as presented above.

B. Illustration and features of the Wigner functions

In Fig. 6, we display the Wigner functions $W_{\Psi,\varepsilon}^\pm(\xi,\eta)$, Eq. (73), and $W_{\Phi,\varepsilon}^\pm$, Eq. (78). These functions depend on the Heaviside step function Θ, Eq. (45), with arguments $\pm\xi$ and $\pm\eta$, respectively. This particular dependency leads to the emergence of horizons in phase space located at $\xi=0$ and $\eta=0$. The domain where the respective Wigner function vanishes is depicted by a white area. In the non-vanishing domain, the value of the Wigner function is governed by the weight function w_ε, Eq. (74). Since the weight function is evaluated at the energy E associated with a respective classical phase space trajectory, the functions $W_{\Psi,\varepsilon}^\pm(\xi,\eta)$ and $W_{\Phi,\varepsilon}^\pm(\xi,\eta)$ attain constant values along these classical trajectories. In Fig. 6, red corresponds to positive and blue to negative weights. The classical trajectories of the inverted harmonic oscillator are also shown in Figs. 1 and 2.

In agreement with Fig. 1, the Wigner functions $W_{\Psi,\varepsilon}^\pm(\xi,\eta)$, depicted in Figs. 6(a) and 6(b), are composed of classical trajectories for particles that propagate *forward* in time and are incoming from the right (+) with initial momentum $p<0$ or left (−) with initial momentum $p>0$. On the other hand, the Wigner functions $W_{\Phi,\varepsilon}^\pm(\xi,\eta)$, displayed in Figs. 6(c) and 6(d), are composed of classical trajectories that correspond to particles that propagate *backwards* in time and are incoming from the right (+) with initial momentum $p>0$ or left (−) with initial momentum $p<0$. While the motion of a classical particle in the inverted oscillator is restricted to a particular trajectory in one of the four quarters of phase space, we emphasize that a quantum particle, as described by the Wigner functions $W_{\Psi,\varepsilon}^\pm(\xi,\eta)$ and $W_{\Phi,\varepsilon}^\pm(\xi,\eta)$, lives on a *half plane* of phase space.

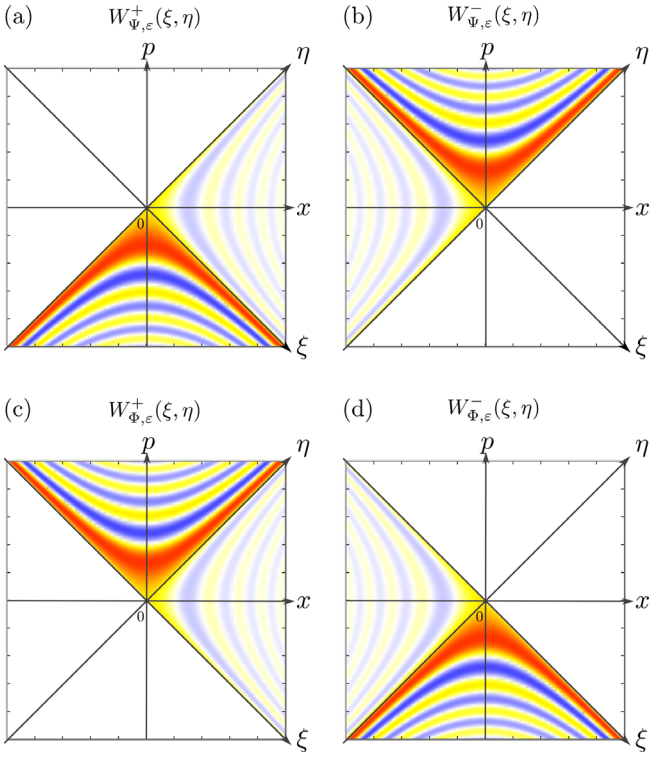

FIG. 6. The Wigner functions $W^{\pm}_{\Psi,\varepsilon}(\xi,\eta)$, Eq. (73), and $W^{\pm}_{\Phi,\varepsilon}(\xi,\eta)$, Eq. (78), corresponding to the energy eigenstates of the inverted harmonic oscillator with dimensionless energy $\varepsilon = 1/2$. Each function occupies a different half plane of phase space restricted by the horizons $\xi = 0$ and $\eta = 0$. Positive and negative values of the Wigner function are depicted by red and blue, respectively. The Wigner functions $W^{\pm}_{\Psi,\varepsilon}(\xi,\eta)$ shown in (a) and (b) are composed of the classical trajectories which belong to incoming particles from the right (+) or left (−) that propagate forward in time. In contrary, the Wigner functions $W^{\pm}_{\Phi,\varepsilon}(\xi,\eta)$ shown in (c) and (d) are composed of the classical trajectories for incoming particles from the right (+) or left (−) that propagate backwards in time. At the horizons $\xi = 0$ and $\eta = 0$, all Wigner functions assume a constant value on the respective half axes.

Next, we explore the particular form of these Wigner functions in more detail. While the Heaviside step function Θ in Eqs. (73) and (78) is evaluated at the phase space variables $\pm\xi$ and $\pm\eta$, respectively, the weight function w_ε, Eq. (74), is governed by the *product* $\xi\eta$. As a consequence, the Wigner functions $W^{\pm}_{\Psi,\varepsilon}(\xi,\eta)$ and $W^{\pm}_{\Phi,\varepsilon}(\xi,\eta)$ are invariant under the simultaneous *dilations*

$$\xi \to \mathrm{e}^{\omega t}\xi \quad \text{and} \quad \eta \to \mathrm{e}^{-\omega t}\eta \tag{79}$$

of phase space for any value of the parameter t.

The transformations presented in Eq. (79) remind of the classical dynamics in the inverted harmonic oscillator, as given by Eqs. (27) and (28) with t corresponding to the time. Indeed, the Wigner functions $W^{\pm}_{\Psi,\varepsilon}(\xi,\eta)$ and $W^{\pm}_{\Phi,\varepsilon}(\xi,\eta)$ maintain their *exact form* during the time evolution in the inverted harmonic oscillator. This feature is characteristic for Wigner functions corresponding to the energy eigenstates of the system under consideration.

In order to underline this property, we consider the action of the dilation operator

$$\widehat{\mathscr{M}}(a,b)\mathscr{F}(\xi,\eta) \equiv \mathscr{F}(a\xi, b\eta) \tag{80}$$

on a phase space function $\mathscr{F}(\xi,\eta)$, resulting in a multiplication of the phase space variables ξ and η by the factors a and b, respectively. For the characteristic Wigner functions of the inverted harmonic oscillator, we then arrive at the relations

$$W^{\pm}_{\Psi,\varepsilon}(\xi,\eta) = \widehat{\mathscr{M}}\left(a^{-1},b^{-1}\right)\widehat{\mathscr{M}}(b,a)W^{\pm}_{\Psi,\varepsilon}(\xi,\eta), \tag{81}$$

or, equivalently,

$$\widehat{\mathscr{M}}(a,b)W^{\pm}_{\Psi,\varepsilon}(\xi,\eta) = \widehat{\mathscr{M}}(b,a)W^{\pm}_{\Psi,\varepsilon}(\xi,\eta), \tag{82}$$

valid for $a, b > 0$. Equations (81) and (82) hold equivalently for the Wigner function $W^{\pm}_{\Phi,\varepsilon}(\xi,\eta)$ and any value of the dimensionless energy ε.

C. The energy dependence of the Wigner functions

Next, we study the dependence of the Wigner function $W^{+}_{\Psi,\varepsilon}(\xi,\eta)$, Eq. (73), on the dimensionless energy ε. For this purpose, we display its shape in Fig. 7 for the dimensionless energies (a) $\varepsilon = -1/2$, (b) $\varepsilon = 1/2$, and (c) $\varepsilon = 0$.

First, we recall that the function $W^{+}_{\Psi,\varepsilon}(\xi,\eta)$ is constant along the classical trajectories of energy E, while its value is provided by the weight function $w_\varepsilon(E)$, Eq. (74). Second, depending on the dimensionless energy ε, the quantum particle is both reflected and transmitted at the potential barrier of an inverted harmonic oscillator. Indeed, the share of the Wigner function in the domain $\eta < 0$ increases as the dimensionless energy ε is increased. Thus, for larger energies ε, it becomes more likely to overcome the parabolic barrier and to enter the domain $x < 0$. Third, the graphs clearly demonstrates that the scattering condition does not allow the particle to pass the horizon $\xi = 0$ in phase space, corresponding to a vanishing Wigner function $W^{+}_{\Psi,\varepsilon}(\xi,\eta)$ in the domain $\xi < 0$.

In order to obtain a deeper insight into the dependence of the Wigner function on the energy ε, we now study the weight function $w_\varepsilon(E)$, Eq. (74), as displayed in Fig. 8. This function provides the weight of each classical trajectories in a half plane of phase space with respect to its energy E as required to construct the Wigner function for the energy ε. We explicitly present the weight function $w_\varepsilon(E)$ for the values $\varepsilon = -1$ (red), $\varepsilon = 0$ (green), and $\varepsilon = 1$ (blue). In particular, for (b) $\varepsilon = 0$, the weight function takes the simple form $w_0(E) = J_0[2E/(\hbar\omega)]$ in terms of the Bessel function J_0.

We emphasize that the weight function $w_\varepsilon(E)$ does not display a sharp peak at the energy $E = \hbar\omega\varepsilon$, indicated by a dashed line of the respective color, as one might expect from the classical situation. In contrary, infinitely many phase space trajectories of different energies compose the corresponding Wigner function.[29] The fact that trajectories of both regimes $E < 0$ and $E > 0$ contribute to the Wigner function manifests itself in the tunneling through the parabolic barrier.[30]

Finally, we note that for large values of the dimensionless energy ε, the Wigner functions $W^{+}_{\Psi,\varepsilon}(\xi,\eta)$ and $W^{-}_{\Phi,\varepsilon}(\xi,\eta)$, as well as $W^{-}_{\Psi,\varepsilon}(\xi,\eta)$ and $W^{+}_{\Phi,\varepsilon}(\xi,\eta)$ become more and more similar while mainly occupying the lower and the upper quadrant of phase space, respectively, as evident from Fig. 6. This observation provides an illustrative explanation for the result presented in Eq. (63). For $\varepsilon \to \infty$, the weights $|S_{\pm}(\varepsilon)|^2$, resembling the Fermi–Dirac statistics, display the behavior $|S_{+}(\varepsilon)|^2 \to 0$ and $|S_{-}(\varepsilon)|^2 \to 1$, according to Eq. (62). As a

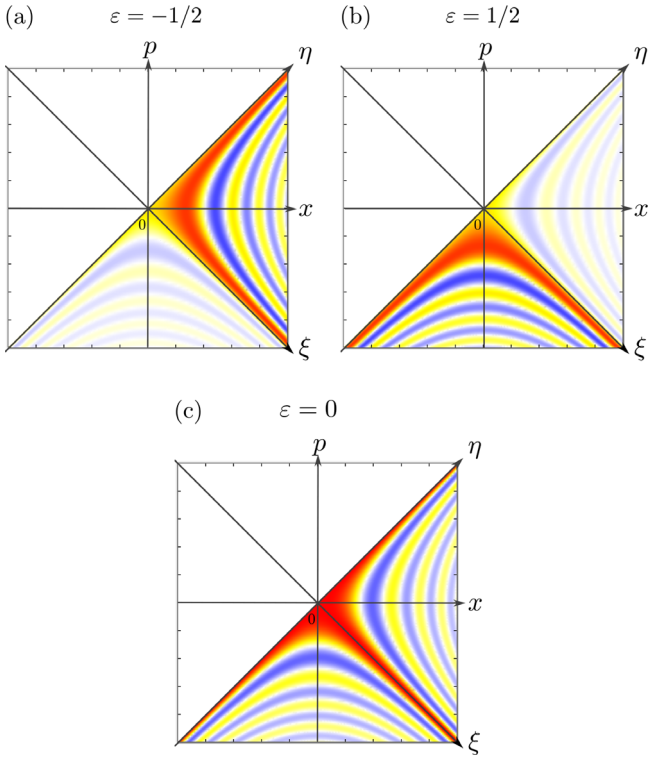

FIG. 7. The Wigner function $W^{+}_{\Psi,\varepsilon}(\xi,\eta)$, Eq. (73), displayed for the dimensionless energies (a) $\varepsilon = -1/2$, (b) $\varepsilon = 1/2$, and (c) $\varepsilon = 0$. In the non-vanishing half plane $\xi \geq 0$, the value of the Wigner function remains constant along the classical phase space trajectories with fixed energy E, as governed by the weight function $w_\varepsilon(E)$, Eq. (74). Positive and negative values are depicted by red and blue, respectively. (a) For a negative energy $\varepsilon < 0$, the major contribution to the Wigner function stems from the right quadrant. Accordingly, a quantum particle incoming from the right is likelier reflected at the potential barrier than transmitted. (b) For a positive energy $\varepsilon > 0$, the transmission through the barrier is more likely. (c) For a vanishing energy $\varepsilon = 0$, transmission and reflection are equally likely.

consequence, the overlap between the states $|\Psi^{+}_{\varepsilon}\rangle$ and $|\Phi^{-}_{\varepsilon}\rangle$ increases for large values of the dimensionless energy ε.

D. The singularity at the horizons in phase space

We are now in the position to explore the emergence of the singularity at the horizons in phase space, as motivated in Secs. III and IV.

On the horizons $\xi = 0$ and $\eta = 0$, the weight function w_ε, Eq. (74), assumes the constant value

$$w_\varepsilon(0) = \frac{1}{\pi}\left[B\left(\frac{1}{2};\frac{1}{2}-\mathrm{i}\varepsilon,\frac{1}{2}+\mathrm{i}\varepsilon\right)+B\left(\frac{1}{2};\frac{1}{2}+\mathrm{i}\varepsilon,\frac{1}{2}-\mathrm{i}\varepsilon\right)\right] \tag{83}$$

corresponding to a vanishing energy $E = 0$, due to the dependence of the energy $E = -\hbar\omega\xi\eta$ on the product $\xi\eta$. Here, B denotes the incomplete Euler beta function. As a consequence of the Heaviside step function Θ, the Wigner functions $W^{\pm}_{\Psi,\varepsilon}(\xi,\eta)$ and $W^{\pm}_{\Phi,\varepsilon}(\xi,\eta)$, given by Eqs. (73) and (78), respectively, either vanish on the horizons or assume the *constant value* $w_\varepsilon(0)$, Eq. (83), on the respective half plane.

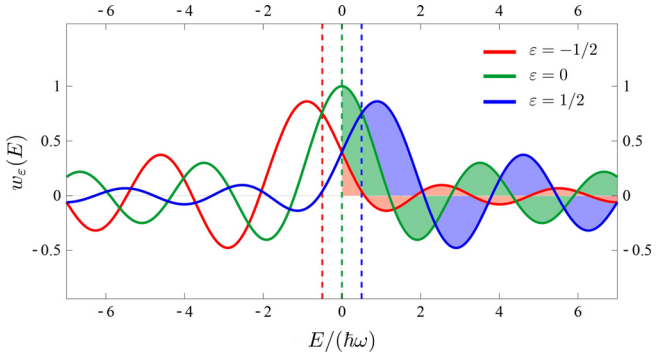

FIG. 8. The weight function $w_\varepsilon(E)$, Eq. (74), yielding the weight for a classical phase space trajectory associated with the energy E to construct the Wigner functions $W^{\pm}_{\Psi,\varepsilon}(\xi,\eta)$, Eq. (73), and $W^{\pm}_{\Phi,\varepsilon}(\xi,\eta)$, Eq. (78), with dimensionless energy ε. We explicitly present the weight functions for the Wigner functions shown in Fig. 7 with $\varepsilon = -1/2$ (red), $\varepsilon = 0$ (green), and $\varepsilon = 1/2$ (blue). While $w_\varepsilon(E)$ displays a large contribution for $E \simeq \hbar\omega\varepsilon$, as indicated by the respective dashed line, we point out that even classical trajectories of different energy E can provide substantial contributions to the respective Wigner function due to the oscillatory behavior of $w_\varepsilon(E)$. According to Eq. (86), the area below the function $w_\varepsilon(E)$ for $E \geq 0$ (depicted by the shaded area) yields the transmission coefficient for the inverted harmonic oscillator. The area in the domain $E \leq 0$ instead provides the reflection coefficient according to Eq. (87). Consequently, the Fermi–Dirac distribution is contained in the weight function $w_\varepsilon(E)$.

In the following, we demonstrate that Eq. (83) also sheds light on the emergence of the amplitude singularity in the energy eigenfunctions $\Psi^{\pm}_{\varepsilon}(\xi)$ and $\Phi^{\pm}_{\varepsilon}(\eta)$, Eqs. (44) and (47), at $\xi = 0$ and $\eta = 0$, respectively. For this purpose, we consider the probability density

$$|\langle\xi|\Psi^{\pm}_{\varepsilon}\rangle|^2 = \int_{-\infty}^{\infty} \mathrm{d}\eta\, W^{\pm}_{\Psi,\varepsilon}(\xi,\eta) \tag{84}$$

obtained as the marginal of the Wigner function $W^{\pm}_{\Psi,\varepsilon}(\xi,\eta)$ by integrating along the η-coordinate, as illustrated in Fig. 9(a).

By inserting the explicit expression Eq. (73) for the Wigner function, the probability density Eq. (84) can be expressed as

$$|\langle\xi|\Psi^{\pm}_{\varepsilon}\rangle|^2 = \frac{\Theta(\pm\xi)}{2\pi\hbar\omega|\xi|}\int_{-\infty}^{\infty} \mathrm{d}E\, w_\varepsilon(E), \tag{85}$$

where we have made use of the substitution $E = -\hbar\omega\xi\eta$.

In Ref. 30, it has been demonstrated that the transmission

$$|S_{-}(\varepsilon)|^2 = \frac{1}{\hbar\omega}\int_{0}^{\infty} \mathrm{d}E\, w_\varepsilon(E) \tag{86}$$

and reflection coefficient

$$|S_{+}(\varepsilon)|^2 = \frac{1}{\hbar\omega}\int_{-\infty}^{0} \mathrm{d}E\, w_\varepsilon(E) \tag{87}$$

of the inverted harmonic oscillator, as defined by Eq. (62), can be obtained by an integral of the weight function $w_\varepsilon(E)$ with regard to positive and negative energies E, respectively. According to Eq. (86), the coefficient $|S_{-}(\varepsilon)|^2$ thus corresponds to the shaded area presented in Fig. 8 for the weight function $w_\varepsilon(E)$.

With the help of the relation $|S_{-}(\varepsilon)|^2 + |S_{+}(\varepsilon)|^2 = 1$, Eq. (64), we then arrive at the probability density

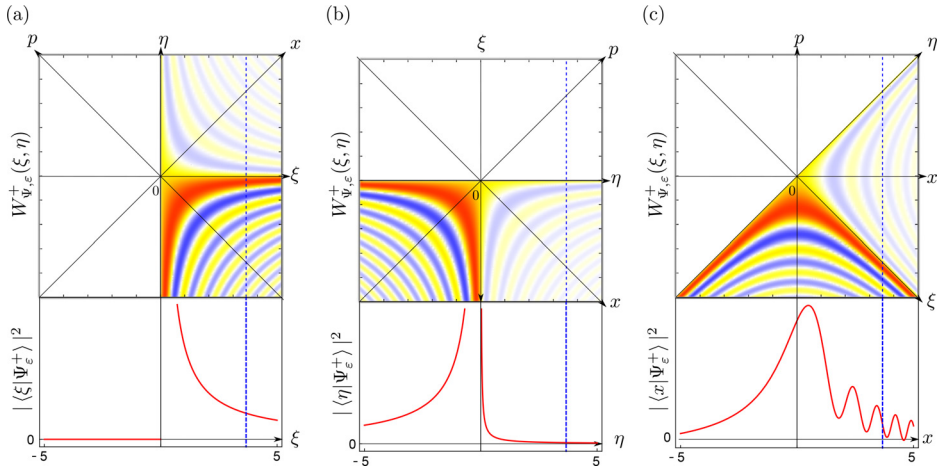

Fig. 9. Projections of the Wigner function $W^+_{\Psi,\varepsilon}(\xi,\eta)$, Eq. (73), for the dimensionless energy $\varepsilon = 1/2$. The respective coordinate of integration is indicated by a blue dashed line. (a) The probability density $|\langle\xi|\Psi^+_\varepsilon\rangle|^2$, Eq. (88), as obtained by integration along the η-coordinate. We clearly observe the emergence of the horizon and the amplitude singularity due to the constant value of the Wigner function $W^+_{\Psi,\varepsilon}(\xi,\eta)$ at the horizon $\xi = 0$. (b) Integration of the Wigner function $W^+_{\Psi,\varepsilon}(\xi,\eta)$ along the ξ-coordinate provides the probability density $|\langle\eta|\Psi^+_\varepsilon\rangle|^2$, Eq. (91). Here, the share for the domains $\eta < 0$ and $\eta > 0$ is governed by the transmission $|S_-(\varepsilon)|^2$ and reflection coefficient $|S_+(\varepsilon)|^2$, respectively, whose dependency on the dimensionless energy ε resembles the Fermi–Dirac statistics according to Eq. (62). (c) Integration of $W^+_{\Psi,\varepsilon}(\xi,\eta)$ along the momentum p provides the probability density $|\langle x|\Psi^+_\varepsilon\rangle|^2$, Eq. (97), in position representation, where neither a horizon nor a singularity are apparent.

$$|\langle\xi|\Psi^\pm_\varepsilon\rangle|^2 = \frac{\Theta(\pm\xi)}{2\pi|\xi|} \tag{88}$$

as obtained from Eqs. (85)–(87) in agreement with Eq. (44) and displayed in Fig. 9(a).

Equations (85)–(88) provide an explanation for the emergence of an amplitude singularity in the wave function $\Psi^\pm_\varepsilon(\xi)$, Eq. (44), caused by the shape of the Wigner function $W^\pm_{\Psi,\varepsilon}(\xi,\eta)$. As stated above, at the horizon, corresponding to a vanishing energy $E = 0$, the Wigner function assumes a constant value in a half plane of phase space. The integration in Eq. (84) with regard to η over the constant value of the Wigner function $W^\pm_{\Psi,\varepsilon}(\xi,\eta)$ for $\xi \to \pm 0$ then leads to the divergence of the wave function $\Psi^\pm_\varepsilon(\xi)$ according to Eq. (88). Thus, it is the presence of a horizon in phase space that causes the amplitude singularity of the wave function $\Psi^\pm_\varepsilon(\xi)$. A similar argument enables the explanation of the amplitude singularity of the wave function $\Phi^\pm_\varepsilon(\eta)$ with the help of the Wigner function $W^\pm_{\Phi,\varepsilon}(\xi,\eta)$.

However, since the Wigner function is bilinear in the wave function, the appearance of the logarithmic phase singularity in the energy eigenfunctions $\Psi^\pm_\varepsilon(\xi)$, Eq. (44), and $\Phi^\pm_\varepsilon(\eta)$, Eq. (47), does not have an obvious correspondence in phase space.

E. The transmission and reflection coefficients resulting from projections of Wigner functions

In Sec. IV C, we have shown that the emergence of the Fermi–Dirac distribution is a consequence of the Fourier transform of a logarithmic phase singularity in combination with a reciprocal square-root singularity of the amplitude. Both features are contained in the ξ-representation of the energy eigenstates $|\Psi^+_\varepsilon\rangle$. In order to demonstrate this intriguing relation, we have considered the probability density $|\langle\eta|\Psi^+_\varepsilon\rangle|^2$, Eq. (63), governed by the state $|\eta\rangle$ and the energy eigenstate $|\Psi^+_\varepsilon\rangle$. In the following, we provide an intuitive geometrical approach that leads to the appearance of a functional dependence that resembles the Fermi–Dirac statistics.

For this purpose, we focus on the marginal

$$|\langle\eta|\Psi^+_\varepsilon\rangle|^2 = \int_{-\infty}^{\infty} \mathrm{d}\xi\, W^+_{\Psi,\varepsilon}(\xi,\eta) \tag{89}$$

of the Wigner function $W^+_{\Psi,\varepsilon}(\xi,\eta)$, Eq. (73), as obtained by the integration along the ξ-coordinate and shown in Fig. 9(b).

Next, we recall that the Wigner function $W^+_{\Psi,\varepsilon}(\xi,\eta)$ is only located in the half plane $\xi > 0$ of phase space. By inserting Eq. (73) in Eq. (89), we thus obtain the integral

$$|\langle\eta|\Psi^+_\varepsilon\rangle|^2 = \frac{1}{2\pi}\int_0^{\infty} \mathrm{d}\xi\, w_\varepsilon(-\hbar\omega\xi\eta), \tag{90}$$

as entirely determined by the weight function w_ε, Eq. (74), in the domain $\xi \geq 0$. With the substitution $E = -\hbar\omega\xi\eta$, we then arrive at the result

$$|\langle\eta|\Psi^+_\varepsilon\rangle|^2 = \frac{1}{2\pi|\eta|}\left[|S_-(\varepsilon)|^2\Theta(-\eta) + |S_+(\varepsilon)|^2\Theta(\eta)\right] \tag{91}$$

coinciding with Eq. (63). Here, we have made use of the dependency of the reflection and transmission coefficients $|S_\pm(\varepsilon)|^2$ on the weight function $w_\varepsilon(E)$ as demonstrated in Eqs. (86) and (87).

Next, we recall the symmetry $|S_-(\varepsilon)|^2 = |S_+(-\varepsilon)|^2$, resulting from Eq. (62) and stating that for the inverted harmonic oscillator the probability of transmission for a quantum particle in the energy eigenstate $|\Psi^+_\varepsilon\rangle$ equals the probability of reflection for the state $|\Psi^+_{-\varepsilon}\rangle$. The same symmetry is reflected in the weight function $w_\varepsilon(E)$ with respect to the line $E = 0$ for $\varepsilon \to -\varepsilon$. In addition, we emphasize that similar to the function $S_\pm(\varepsilon)$, Eq. (56), the weight function $w_\varepsilon(E)$, Eq. (74), also results from a Fourier transform of an amplitude singularity in combination with a logarithmic phase singularity. However, here two singular points arise at the boundaries of the integration region.

In summary, the coefficients $|S_\pm(\varepsilon)|^2$, resembling a Fermi–Dirac distribution, can be obtained by integrating the Wigner function

$W^{+}_{\Psi,\varepsilon}(\xi,\eta)$ along the ξ-coordinate for a fixed value of η. Here, $\eta<0$ yields $|S_{-}(\varepsilon)|^2$ and $\eta>0$ provides $|S_{+}(\varepsilon)|^2$ together with the prefactor $(2\pi|\eta|)^{-1}$, as demonstrated in Eq. (89). We emphasize that this procedure yields the respective transmission $|S_{-}(\varepsilon)|^2$ and reflection coefficient $|S_{+}(\varepsilon)|^2$ for a Wigner function $W^{+}_{\Psi,\varepsilon}(\xi,\eta)$ with a *specific* dimensionless energy ε. By repeating this approach for Wigner functions $W^{+}_{\Psi,\varepsilon}(\xi,\eta)$ corresponding to *different* energies ε, it is possible to reconstruct the Fermi–Dirac statistics with the help of these phase space distributions.

F. The spatial probability density resulting from a projection of the Wigner function

Finally, we demonstrate that the probability distribution of an energy eigenstate of the inverted harmonic oscillator in position representation can also be extracted from the respective Wigner function. In Sec. IV D, we have shown that the horizons and singularities are not present in this particular representation. We now explore the reasons for their disappearance.

For this purpose, we consider the Wigner function

$$W_x(\xi,\eta)=\frac{1}{2\pi}\int_{-\infty}^{\infty}\mathrm{d}y\,\mathrm{e}^{-\mathrm{i}\eta y}\left\langle x\middle|\xi-\frac{y}{2}\right\rangle\left\langle\xi+\frac{y}{2}\middle|x\right\rangle \tag{92}$$

corresponding to a position eigenstate $|x\rangle$. By making use of the position representation

$$\langle x|\xi\rangle=\frac{1}{\sqrt{\pi}}\left(\frac{m\omega}{2\hbar}\right)^{1/4}\mathrm{e}^{\mathrm{i}\left(\frac{m\omega}{2\hbar}x^2-\sqrt{\frac{2m\omega}{\hbar}}x\xi+\frac{\xi^2}{2}\right)-\mathrm{i}\frac{\pi}{8}} \tag{93}$$

of the state $|\xi\rangle$, as derived in Appendix A, we evaluate the integral in Eq. (92). As a result, the Wigner function takes the form

$$W_x(\xi,\eta)=\frac{1}{2\pi}\sqrt{\frac{2m\omega}{\hbar}}\delta\left(\eta+\xi-\sqrt{\frac{2m\omega}{\hbar}}x\right) \tag{94}$$

corresponding to the line $\eta+\xi=\sqrt{2m\omega/\hbar}x$ in phase space with regard to a specific value of x, as displayed by the blue dashed line in Fig. 9(c).

Next, we express the probability density $|\psi^{+}_{\varepsilon}(x)|^2$ in position representation, which is determined by the wave function $\psi^{+}_{\varepsilon}(x)=\langle x|\Psi^{+}_{\varepsilon}\rangle$, Eq. (65), as the overlap[51]

$$|\langle x|\Psi^{+}_{\varepsilon}\rangle|^2=2\pi\int_{-\infty}^{\infty}\mathrm{d}\xi\int_{-\infty}^{\infty}\mathrm{d}\eta\,W^{+}_{\Psi,\varepsilon}(\xi,\eta)W_x(\xi,\eta) \tag{95}$$

of the Wigner functions $W^{+}_{\Psi,\varepsilon}(\xi,\eta)$ and $W_x(\xi,\eta)$ in phase space. The overlap presented in Eq. (95) actually corresponds to the marginal

$$|\langle x|\Psi^{+}_{\varepsilon}\rangle|^2=\int_{-\infty}^{\infty}\mathrm{d}p\,W^{+}_{\Psi,\varepsilon}[\xi(x,p),\eta(x,p)] \tag{96}$$

shown in Fig. 9(c), as obtained by inserting the explicit form of the Wigner function $W_x(\xi,\eta)$, Eq. (92), in Eq. (95). Here, we have expressed the variables $\xi=\xi(x,p)$ and $\eta=\eta(x,p)$ by the position x and the momentum p according to Eqs. (20) and (21). This result confirms the invariance of the Wigner function under canonical transformations as pointed out in the beginning of this section.

Utilizing the explicit expression Eq. (73) for the Wigner function $W^{+}_{\Psi,\varepsilon}(\xi,\eta)$ then yields the result

$$|\langle x|\Psi^{+}_{\varepsilon}\rangle|^2=\frac{1}{2\pi}\int_{-\infty}^{m\omega x}\mathrm{d}p\,w_{\varepsilon}\left(\frac{p^2}{2m}-\frac{1}{2}m\omega^2x^2\right). \tag{97}$$

Consequently, not only the Fermi–Dirac distribution, as resulting from Eqs. (86) and (87), but also the probability density $|\psi^{+}_{\varepsilon}(x)|^2$ for the wave function $\psi^{+}_{\varepsilon}(x)$, Eq. (65), in position representation can be obtained from the weight function w_{ε}, Eq. (74).

As shown in Fig. 9(c), there is no horizon or singularity present in the probability density $|\langle x|\Psi^{+}_{\varepsilon}\rangle|^2$ in position representation. The reason for the disappearance of these features can be found in the direction of integration of the corresponding phase distribution in Eq. (96). Indeed, the momentum p is neither parallel to the horizon $\xi=0$ nor to the horizon $\eta=0$. Thus, there is no integration over a constant value which would have led to a singularity as discussed in Sec. V D.

Moreover, Eq. (96) also hints at an illustrative explanation for Stokes phenomenon and the different asymptotic expansions of the wave function $\psi^{+}_{\varepsilon}(x)$, Eq. (65), presented in Eqs. (68) and (69) for $x\gg1$ and $x\ll-1$, respectively. For this purpose, we consider the corresponding Wigner function $W^{+}_{\Psi,\varepsilon}(\xi,\eta)$ displayed in Fig. 9(c).

For $x>0$, there are contributions to the integral in Eq. (97) which stem from the two domains $\eta>0$ and $\eta<0$, being separated by the horizon $\eta=0$ in phase space. As a consequence, the corresponding asymptotic expansion Eq. (68) is composed of the sum of two terms.

On the other hand, in the domain $x<0$ only the contributions for $\eta<0$ contributes to the integral in Eq. (97). Consequently, the asymptotic expansion for $x\ll-1$ in Eq. (69) contains only a single term.

It is intriguing that this illustrative description in terms of Wigner functions establishes a relationship between the *horizons in phase space* and the *Stokes phenomenon* of complex analysis.

VI. SUMMARY AND OUTLOOK

In the present article, we have investigated the inverted harmonic oscillator both from a classical and a quantum perspective. In particular, we have explored similarities and differences between this system and the physics of Hawking radiation emitted by a black hole.

We have demonstrated that the dynamics and kinematics in the inverted oscillator are strongly influenced by the presence of two horizons. In contrast to a black hole, displaying an event horizon in spacetime, the horizons of the inverted harmonic oscillator are located in phase space. At these horizons, a logarithmic phase singularity of the energy eigenfunctions emerges, whose origin is to be found in the classical domain. Indeed, the mode functions of a massless scalar field also display a logarithmic phase singularity at the event horizon of a black hole.

The phase singularity of the inverted harmonic oscillator is accompanied by an amplitude singularity that manifests itself in a reciprocal square-root dependence on the coordinate. However, at the event horizon of a black hole, such an amplitude singularity is absent in the mode functions of a quantized bosonic field. This pure logarithmic phase singularity leads to the emergence of a Bose–Einstein statistics governing the number of particles emitted via Hawking radiation. This result is in contrast to the inverted harmonic oscillator, where the transmission and reflection coefficients are reminiscent of the Fermi–Dirac statistics. We have demonstrated that this particular dependency is a consequence of the Fourier transform of a function that displays a logarithmic phase singularity in combination with a particular amplitude singularity. Moreover, we have shown that in the position representation of quantum mechanics these particular

features of the inverted harmonic oscillator are hidden and only remnants are visible.

In order to obtain a deeper insight into these phenomena, we have analyzed the Wigner function as an illustrative phase space representation for the energy eigenstates of the inverted harmonic oscillator. In particular, we have shown that the horizons in phase space crucially determine the shape of these functions. Our approach provides a simple explanation for the emergence of the horizons in phase space and the amplitude singularity due to a dependence of the Wigner function on the product $\xi\eta$ of the phase space coordinates ξ and η. In this regard, we have also analyzed the invariance of these Wigner functions with regard to specific dilations of the phase space coordinates. While these features yield an intuitive geometric explanation for the horizons and the amplitude singularity, such a simple picture for the appearance of the logarithmic phase singularity in the energy eigenfunctions remains to be found. Beyond that, we have demonstrated the relation between particular projections of the Wigner function and the Fermi–Dirac distribution, as well as the connection between the horizons in phase space and the Stokes phenomenon.

In conclusion, we have established intriguing relationships between the physics of Hawking radiation and the elementary system of a quantum particle exposed to an inverted harmonic oscillator. Central to our analogy are the emergence of horizons in combination with a logarithmic phase singularity.

It would be intriguing to perform an experimental demonstration of the horizons intrinsic to the system of an inverted harmonic oscillator. A possible physical system for this purpose are surface gravity water waves, which behave in the linear regime analogous to Schrödinger waves with time and space coordinates being interchanged. Moreover, these waves enable the extraction of phases that are accumulated with regard to a carrier wave.[52] Such an experiment might thus strengthen the intimidate relationship between the model of an inverted harmonic oscillator and Hawking radiation emitted by a black hole, manifesting itself in the appearance of a particular quantum statistics due to a logarithmic phase singularity.

We point out that the logarithmic phase in the inverted harmonic oscillator belongs to a larger class of phases that are characteristic for particular quantum systems. Indeed, the logarithmic phase is closely related to the Gouy phase[53] as accumulated during the free propagation of a Gaussian wave packet or, more generally, an energy eigenstate of a harmonic potential. However, not only quadratic potentials but also linear potentials feature particular quantum mechanical phases of interest. As a particular example, the so-called Kennard phase[52,54–56] has been studied with regard to the equivalence principle and the Unruh effect within the context of gravitizing quantum mechanics.[57,58] Maybe these simple quantum systems may enable us to obtain a deeper insight into the phenomena that occur at the interface of quantum mechanics and general relativity.

ACKNOWLEDGMENTS

The authors acknowledge fruitful discussions with A. Arie, W. B. Case, and G. G. Rozenman. In particular, we are grateful to M. A. Efremov for his valuable remarks.

AUTHOR DECLARATIONS

Conflict of Interest

The authors have no conflicts to disclose.

DATA AVAILABILITY

The data that support the findings of this study are available within the article.

APPENDIX A: POSITION REPRESENTATION OF THE STATES $|\xi\rangle$ AND $|\eta\rangle$

In this appendix, we determine the position representation of the states $|\xi\rangle$ and $|\eta\rangle$. These states have been introduced in Sec. IV A as eigenstates of the operators

$$\hat{\xi} = \sqrt{\frac{m\omega}{2\hbar}}\left(\hat{x} - \frac{\hat{p}}{m\omega}\right) \tag{A1}$$

and

$$\hat{\eta} = \sqrt{\frac{m\omega}{2\hbar}}\left(\hat{x} + \frac{\hat{p}}{m\omega}\right), \tag{A2}$$

with eigenvalues ξ and η, respectively.

First, we consider the position $\hat{x}$ and momentum $\hat{p}$ operator in the Heisenberg picture

$$\hat{x}_{\mathrm{H}}(t) \equiv \hat{U}^{\dagger}_{\mathrm{HO}}(t)\hat{x}\hat{U}_{\mathrm{HO}}(t), \tag{A3}$$

$$\hat{p}_{\mathrm{H}}(t) \equiv \hat{U}^{\dagger}_{\mathrm{HO}}(t)\hat{p}\hat{U}_{\mathrm{HO}}(t), \tag{A4}$$

at time t, as determined by the time-evolution operator

$$\hat{U}_{\mathrm{HO}}(t) = \exp\left(-\frac{\mathrm{i}}{\hbar}\hat{H}_{\mathrm{HO}}t\right) \tag{A5}$$

corresponding to the Hamiltonian

$$\hat{H}_{\mathrm{HO}} = \frac{\hat{p}^2}{2m} + \frac{1}{2}m\omega^2\hat{x}^2 \tag{A6}$$

of a harmonic oscillator with frequency ω.

By solving the Heisenberg equations of motion

$$\frac{\mathrm{d}}{\mathrm{d}t}\hat{x}_{\mathrm{H}}(t) = \frac{\hat{p}_{\mathrm{H}}(t)}{m}, \tag{A7}$$

$$\frac{\mathrm{d}}{\mathrm{d}t}\hat{p}_{\mathrm{H}}(t) = -m\omega^2\hat{x}_{\mathrm{H}}(t), \tag{A8}$$

we obtain the position operator

$$\hat{x}_{\mathrm{H}}(t) = \hat{x}\cos(\omega t) + \frac{\hat{p}}{m\omega}\sin(\omega t), \tag{A9}$$

and the momentum operator

$$\hat{p}_{\mathrm{H}}(t) = \hat{p}\cos(\omega t) - m\omega\hat{x}\sin(\omega t), \tag{A10}$$

as defined by Eqs. (A3) and (A4), respectively. Here, we have made use of the initial conditions $\hat{x}_{\mathrm{H}}(0) = \hat{x}$ and $\hat{p}_{\mathrm{H}}(0) = \hat{p}$.

Thus, according to Eqs. (A1) and (A2) the operators

$$\hat{\xi} = \sqrt{\frac{m\omega}{\hbar}}\hat{x}_{\mathrm{H}}\left(-\frac{\pi}{4\omega}\right) \tag{A11}$$

and

$$\hat{\eta} = \sqrt{\frac{m\omega}{\hbar}}\hat{x}_{\mathrm{H}}\left(\frac{\pi}{4\omega}\right) \tag{A12}$$

are governed by the position operator $\hat{x}_{\mathrm{H}}(t)$, Eq. (A9), in the Heisenberg picture with regard to the harmonic oscillator and evaluated at the times $t = -\pi/(4\omega)$ and $t = \pi/(4\omega)$, respectively.

Next, we turn to the eigenvalue equation

$$\hat{\xi}|\xi\rangle = \xi|\xi\rangle \tag{A13}$$

for the operator $\hat{\xi}$, Eq. (A1), and the eigenstate $|\xi\rangle$ with eigenvalue ξ. By making use of Eqs. (A3) and (A11), we recast Eq. (A13) in the form

$$\hat{x}|x_\xi^-\rangle = x_\xi^-|x_\xi^-\rangle, \tag{A14}$$

where the eigenstate

$$|x_\xi^-\rangle \equiv \mathcal{N}_\xi^- \hat{U}_{\mathrm{HO}}\left(-\frac{\pi}{4\omega}\right)|\xi\rangle \tag{A15}$$

of the position operator $\hat{x}$ with normalization constant $\mathcal{N}_\xi^-$ corresponds to the eigenvalue

$$x_\xi^- = \sqrt{\frac{\hbar}{m\omega}}\xi. \tag{A16}$$

Analogously, we consider the eigenvalue equation

$$\hat{\eta}|\eta\rangle = \eta|\eta\rangle \tag{A17}$$

for the operator $\hat{\eta}$, Eq. (A2), and the eigenstate $|\eta\rangle$ with eigenvalue η. With the help of Eqs. (A12) and (A17), we then establish the relation between the state $|\eta\rangle$ and the position eigenstate

$$|x_\eta^+\rangle \equiv \mathcal{N}_\eta^+ \hat{U}_{\mathrm{HO}}\left(\frac{\pi}{4\omega}\right)|\eta\rangle, \tag{A18}$$

with normalization constant $\mathcal{N}_\eta^+$ and eigenvalue

$$x_\eta^+ = \sqrt{\frac{\hbar}{m\omega}}\eta. \tag{A19}$$

We determine the normalization constants $\mathcal{N}_\xi^-$ and $\mathcal{N}_\eta^+$ in Eqs. (A16) and (A18), respectively. For this purpose, we consider the scalar product

$$\langle\xi|\eta\rangle = \frac{1}{\sqrt{2\pi}}\exp\left(\mathrm{i}\xi\eta\right) \tag{A20}$$

of the states $|\xi\rangle$ and $|\eta\rangle$. By making use of Eqs. (A15) and (A18), we are able to express this scalar product

$$\langle\xi|\eta\rangle = \left[\mathcal{N}_\eta^+\left(\mathcal{N}_\xi^-\right)^*\right]^{-1}\left\langle x_\xi^-\middle|\hat{U}_{\mathrm{HO}}\left(-\frac{\pi}{2\omega}\right)\middle|x_\eta^+\right\rangle \tag{A21}$$

in terms of the matrix element of the time-evolution operator $\hat{U}_{\mathrm{HO}}(t)$, Eq. (A5), with respect to the position eigenstates $|x_\xi^-\rangle$ and $|x_\eta^+\rangle$, evaluated at time $t = -\pi/(2\omega)$.

Next, we recall the Mehler kernel[59]

$$\langle x|\hat{U}_{\mathrm{HO}}(t)|y\rangle = \sqrt{\frac{m\omega}{2\pi\mathrm{i}\hbar\sin\left(\omega t\right)}}\mathrm{e}^{\frac{\mathrm{i}m\omega\left[\left(x^2+y^2\right)\cos\left(\omega t\right)-2xy\right]}{2\hbar\sin\left(\omega t\right)}} \tag{A22}$$

for the position eigenstates $|x\rangle$ and $|y\rangle$ in order to evaluate the matrix element

$$\left\langle x_\xi^-\middle|\hat{U}_{\mathrm{HO}}\left(-\frac{\pi}{2\omega}\right)\middle|x_\eta^-\right\rangle = \sqrt{\frac{m\omega}{2\pi\hbar}}\mathrm{e}^{\mathrm{i}\pi/4}\exp\left(\mathrm{i}\xi\eta\right) \tag{A23}$$

in Eq. (A21), where we have made use of Eqs. (A16) and (A19). We insert Eq. (A23) in Eq. (A21), and compare Eq. (A20) with Eq. (A21) to identify the product

$$\mathcal{N}_\eta^+\left(\mathcal{N}_\xi^-\right)^* = \sqrt{\frac{\hbar}{m\omega}}\mathrm{e}^{\mathrm{i}\pi/4} \tag{A24}$$

of the normalization constants $\mathcal{N}_\eta^+$ and $\mathcal{N}_\xi^-$.

Moreover, with Eqs. (A15) and (A16), we arrive at the orthogonality relation

$$\langle x_{\xi'}^-|x_\xi^-\rangle = \sqrt{\frac{m\omega}{\hbar}}\delta(\xi-\xi') = \left(\mathcal{N}_{\xi'}^-\right)^*\mathcal{N}_\xi^-\langle\xi'|\xi\rangle \tag{A25}$$

for the position eigenstates $|x_\xi^-\rangle$ and $|x_{\xi'}^-\rangle$. With Eqs. (A18) and (A19) we also obtain the orthogonality relation

$$\langle x_{\eta'}^+|x_\eta^+\rangle = \sqrt{\frac{m\omega}{\hbar}}\delta(\eta-\eta') = \left(\mathcal{N}_{\eta'}^+\right)^*\mathcal{N}_\eta^+\langle\eta'|\eta\rangle \tag{A26}$$

for the position eigenstates $|x_{\eta'}^+\rangle$ and $|x_\eta^+\rangle$.

We make use of the orthogonality relations

$$\langle\xi'|\xi\rangle = \delta(\xi-\xi') \text{ and } \langle\eta'|\eta\rangle = \delta(\eta-\eta'), \tag{A27}$$

and determine in agreement with Eqs. (A23), (A25), and (A26) the normalization constants

$$\mathcal{N}_\xi^- = \left(\frac{m\omega}{\hbar}\right)^{1/4}\mathrm{e}^{-\mathrm{i}\pi/8} \tag{A28}$$

in Eq. (A15), and

$$\mathcal{N}_\eta^+ = \left(\frac{m\omega}{\hbar}\right)^{1/4}\mathrm{e}^{\mathrm{i}\pi/8} \tag{A29}$$

in Eq. (A18) up to an identical overall phase factor.

Finally, we turn to the position-representation of the quasi-coherent states $|\xi\rangle$ and $|\eta\rangle$. For this purpose, we make use of Eqs. (A15) and (A18) to obtain the expressions

$$\langle x|\xi\rangle = \frac{1}{\mathcal{N}_\xi^-}\left\langle x\middle|\hat{U}_{\mathrm{HO}}\left(\frac{\pi}{4\omega}\right)\middle|x_\xi^-\right\rangle \tag{A30}$$

and

$$\langle x|\eta\rangle = \frac{1}{\mathcal{N}_\eta^+}\left\langle x\middle|\hat{U}_{\mathrm{HO}}\left(-\frac{\pi}{4\omega}\right)\middle|x_\eta^+\right\rangle. \tag{A31}$$

By inserting Eq. (A15) in Eq. (A30) and evaluating the Mehler kernel, Eq. (A22), at time $t = \pi/(4\omega)$, and position $y = x_\xi^-$, Eq. (A30), we arrive at the position representation

$$\langle x|\xi\rangle = \frac{1}{\sqrt{\pi}}\left(\frac{m\omega}{2\hbar}\right)^{1/4}\mathrm{e}^{\mathrm{i}\left(\frac{m\omega}{2\hbar}x^2-\sqrt{\frac{2m\omega}{\hbar}}x\xi+\frac{\xi^2}{2}\right)-\mathrm{i}\frac{\pi}{8}} \tag{A32}$$

of the state $|\xi\rangle$.

Similarly, we insert Eq. (A29) in Eq. (A31) and evaluate Eq. (A22) at time $t = -\pi/(4\omega)$ and position $y = x_\eta^+$, Eq. (A19), to obtain the position representation

$$\langle x|\eta\rangle = \frac{1}{\sqrt{\pi}}\left(\frac{m\omega}{2\hbar}\right)^{1/4} \mathrm{e}^{-\mathrm{i}\left(\frac{m\omega}{2\hbar}x^2 - \sqrt{\frac{2m\omega}{\hbar}}x\eta + \frac{\eta^2}{2}\right) + \mathrm{i}\frac{\pi}{8}} \tag{A33}$$

of the state $|\eta\rangle$.

APPENDIX B: POSITION REPRESENTATION OF THE ENERGY EIGENSTATES $|\Psi_\varepsilon^\pm\rangle$ AND $|\Phi_\varepsilon^\pm\rangle$

In the following, we derive the position representation of the energy eigenstates $|\Psi_\varepsilon^\pm\rangle$ and $|\Phi_\varepsilon^\pm\rangle$ of the inverted harmonic oscillator for the dimensionless energy ε.

According to Sec. IV B, these eigenstates are characterized by the ξ-representation

$$\langle\xi|\Psi_\varepsilon^\pm\rangle = \frac{1}{\sqrt{2\pi|\xi|}}\exp\left(-\mathrm{i}\varepsilon\ln|\xi|\right)\Theta(\pm\xi), \tag{B1}$$

and η-representation

$$\langle\eta|\Phi_\varepsilon^\pm\rangle = \frac{1}{\sqrt{2\pi|\eta|}}\exp\left(\mathrm{i}\varepsilon\ln|\eta|\right)\Theta(\pm\eta), \tag{B2}$$

respectively.

In order to obtain the position representation $\psi_\varepsilon^\pm(x) \equiv \langle x|\Psi_\varepsilon^\pm\rangle$, we make use of the identity

$$\mathbb{1} = \int_{-\infty}^{\infty}\mathrm{d}\xi|\xi\rangle\langle\xi| \tag{B3}$$

for the states $|\xi\rangle$. Consequently, the position representation of the energy eigenstate $|\Psi_\varepsilon^\pm\rangle$ can be expressed as the integral

$$\psi_\varepsilon^\pm(x) = \int_{-\infty}^{\infty}\mathrm{d}\xi\,\langle x|\xi\rangle\langle\xi|\Psi_\varepsilon^\pm\rangle. \tag{B4}$$

Next, we focus on the positive sign in Eq. (B4) and insert the ξ-representation of the energy eigenstate $|\Psi_\varepsilon^+\rangle$, Eq. (B1), as well as the position representation of the state $|\xi\rangle$, Eq. (A32), which yields the Mellin transform

$$\psi_\varepsilon^+(x) = \frac{1}{\sqrt{2\pi}}\left(\frac{m\omega}{2\hbar}\right)^{1/4}\mathrm{e}^{-\mathrm{i}\pi/8}\int_0^\infty\mathrm{d}\xi\,\xi^{-\frac{1}{2}-\mathrm{i}\varepsilon}\mathrm{e}^{\mathrm{i}\left(\frac{m\omega}{2\hbar}x^2 - \sqrt{\frac{2m\omega}{\hbar}}x\xi + \frac{\xi^2}{2}\right)}. \tag{B5}$$

By making use of the relation[60]

$$D_s\left(\frac{b}{\sqrt{2a}}\right) = \frac{(2a)^{-s/2}}{\Gamma(-s)}\int_0^\infty\mathrm{d}\xi\,\xi^{-s-1}\mathrm{e}^{-a\xi^2 - b\xi - \frac{b^2}{8a}} \tag{B6}$$

for the parabolic cylinder function D_s[49] with the parameters $a \equiv -\mathrm{i}/2$, $b \equiv \mathrm{i}x\sqrt{2m\omega/\hbar}$, and $s \equiv -1/2 + \mathrm{i}\varepsilon$, we then arrive at the position representation

$$\psi_\varepsilon^+(x) = \frac{\Gamma\left(\frac{1}{2} - \mathrm{i}\varepsilon\right)}{\sqrt{2\pi}}\left(\frac{m\omega}{2\hbar}\right)^{1/4}\mathrm{e}^{\varepsilon\pi/4}D_{-\frac{1}{2}+\mathrm{i}\varepsilon}\left(\mathrm{e}^{\mathrm{i}3\pi/4}\sqrt{\frac{2m\omega}{\hbar}}x\right) \tag{B7}$$

of the energy eigenstate $|\Psi_\varepsilon^+\rangle$.

With the help of the symmetry relation $\langle x| - \xi\rangle = \langle -x|\xi\rangle$ of the scalar product presented in Eq. (A32), we immediately obtain the position representation

$$\psi_\varepsilon^-(x) = \psi_\varepsilon^+(-x) \tag{B8}$$

of the energy eigenstate $|\Psi_\varepsilon^-\rangle$ with negative sign according to Eqs. (B1) and (B4).

Next, we turn to the position representation $\phi_\varepsilon^\pm(x) \equiv \langle x|\Phi_\varepsilon^\pm\rangle$ of the energy eigenstates $|\Phi_\varepsilon^\pm\rangle$. Here, we make use of the identity

$$\mathbb{1} = \int_{-\infty}^{\infty}\mathrm{d}\eta|\eta\rangle\langle\eta| \tag{B9}$$

in order to arrive at the expression

$$\phi_\varepsilon^\pm(x) = \int_{-\infty}^{\infty}\mathrm{d}\eta\,\langle x|\eta\rangle\langle\eta|\Phi_\varepsilon^\pm\rangle. \tag{B10}$$

We note that both scalar products $\langle x|\eta\rangle$, Eq. (A33), and $\langle\eta|\Phi_\varepsilon^\pm\rangle$, Eq. (B2), correspond to the complex conjugate of the expressions $\langle x|\xi\rangle$, Eq. (A32), and $\langle\xi|\Psi_\varepsilon^\pm\rangle$, Eq. (B1), respectively, when replacing the variable ξ by η.

With the help of Eqs. (B4) and (B10), we thus establish the relation

$$\phi_\varepsilon^\pm(x) = \left[\psi_\varepsilon^\pm(x)\right]^*. \tag{B11}$$

Our results can be summarized by the explicit expressions

$$\psi_\varepsilon^\pm(x) = \frac{\Gamma\left(\frac{1}{2} - \mathrm{i}\varepsilon\right)}{\sqrt{2\pi}}\left(\frac{m\omega}{2\hbar}\right)^{1/4}\mathrm{e}^{\varepsilon\pi/4}D_{-\frac{1}{2}+\mathrm{i}\varepsilon}\left(\pm\mathrm{e}^{\mathrm{i}3\pi/4}\sqrt{\frac{2m\omega}{\hbar}}x\right) \tag{B12}$$

for the position representation of the energy eigenstate $|\Psi_\varepsilon^\pm\rangle$ according to Eqs. (B7) and (B8), and

$$\phi_\varepsilon^\pm(x) = \frac{\Gamma\left(\frac{1}{2} + \mathrm{i}\varepsilon\right)}{\sqrt{2\pi}}\left(\frac{m\omega}{2\hbar}\right)^{1/4}\mathrm{e}^{\varepsilon\pi/4}D_{-\frac{1}{2}-\mathrm{i}\varepsilon}\left(\pm\mathrm{e}^{-\mathrm{i}3\pi/4}\sqrt{\frac{2m\omega}{\hbar}}x\right) \tag{B13}$$

for the position representation of the energy eigenstate $|\Phi_\varepsilon^\pm\rangle$ according to Eqs. (B11) and (B12).

REFERENCES

[1] R. Penrose, Phys. Rev. Lett. **14**, 57 (1965).
[2] A. Einstein, Sitzungsber. Preuss. Akad. Wiss. **1915**, 844; reprinted in *Albert Einstein: Akademie-Vorträge*, edited by D. Simon (Wiley, Hoboken, NJ, 2005).
[3] R. Genzel, F. Eisenhauer, and S. Gillessen, Rev. Mod. Phys. **82**, 3121 (2010).
[4] B. P. Abbott *et al.*, Phys. Rev. Lett. **116**, 061102 (2016).
[5] S. Hawking, Nature **248**, 30 (1974).
[6] W. Rindler, Phys. Rev. **119**, 2082 (1960).
[7] R. Brout, S. Massar, R. Parentani, and P. Spindel, Phys. Rep. **260**, 329 (1995).
[8] W. G. Unruh, Phys. Rev. D **14**, 870 (1976).
[9] G. Agarwal *et al.*, J. Mod. Opt. **65**, 1261 (2018).
[10] M. Scully, S. Fulling, D. Lee, D. Page, W. Schleich, and A. Svidzinsky, Proc. Natl. Acad. Sci. U. S. A. **115**, 8131 (2018).
[11] J. S. Ben-Benjamin, M. O. Scully, S. A. Fulling, D. M. Lee, D. N. Page, A. A. Svidzinsky, M. S. Zubairy, M. J. Duff, R. Glauber *et al.*, Int. J. Mod. Phys. A **34**, 1941005 (2019).

[12]P. Betzios, N. Gaddam, and O. Papadoulaki, "Black holes, quantum chaos, and the Riemann hypothesis," arXiv:2004.09523 (2020).
[13]V. Subramanyan, S. S. Hegde, S. Vishveshwara, and B. Bradlyn, Ann. Phys. **435**, 168470 (2021).
[14]S. S. Hegde, V. Subramanyan, B. Bradlyn, and S. Vishveshwara, Phys. Rev. Lett. **123**, 156802 (2019).
[15]M. V. Berry and J. P. Keating, "H = xp and the Riemann zeros," in *NATO ASI Series* (Springer US, Boston, MA, 1999), pp. 355–367.
[16]C. Barceló, S. Liberati, and M. Visser, Living Rev. Relativ. **14**, 3 (2011).
[17]S. J. Robertson, J. Phys. B **45**, 163001 (2012).
[18]W. G. Unruh, Phys. Rev. Lett. **46**, 1351 (1981).
[19]Y. Rosenberg, Philos. Trans. R. Soc. A **378**, 20190232 (2020).
[20]U. Leonhardt, Nature **415**, 406 (2002).
[21]U. Leonhardt, Phys. Rev. A **65**, 043818 (2002).
[22]J. Steinhauer, Nat. Phys. **10**, 864 (2014).
[23]J. Steinhauer, Nat. Phys. **12**, 959 (2016).
[24]C. Gooding, S. Biermann, S. Erne, J. Louko, W. G. Unruh, J. Schmiedmayer, and S. Weinfurtner, Phys. Rev. Lett. **125**, 213603 (2020).
[25]S. Weinfurtner, E. W. Tedford, M. C. J. Penrice, W. G. Unruh, and G. A. Lawrence, Phys. Rev. Lett. **106**, 021302 (2011).
[26]S. Patrick, H. Goodhew, C. Gooding, and S. Weinfurtner, Phys. Rev. Lett. **126**, 041105 (2021).
[27]P. Betzios, N. Gaddam, and O. Papadoulaki, J. High Energy Phys. **2016**, 131.
[28]T. Morita, Phys. Rev. Lett. **122**, 101603 (2019).
[29]N. Balazs and A. Voros, Ann. Phys. **199**, 123 (1990).
[30]D. Heim, W. Schleich, P. Alsing, J. Dahl, and S. Varro, Phys. Lett. A **377**, 1822 (2013).
[31]G. Barton, Ann. Phys. **166**, 322 (1986).
[32]D. Bermudez and D. Fernández C., Ann. Phys. **333**, 290 (2013).
[33]S. Nonnenmacher and A. Voros, J. Phys. A **30**, 295 (1997).
[34]G. 'T Hooft, Int. J. Mod. Phys. A **11**, 4623 (1996).
[35]M. K. Parikh and F. Wilczek, Phys. Rev. Lett. **85**, 5042 (2000).
[36]E. C. Kemble, Phys. Rev. **48**, 549 (1935).
[37]W. Heisenberg and H. Euler, Z. Phys. **98**, 714 (1936).
[38]J. Schwinger, Phys. Rev. **82**, 664 (1951).
[39]R. Parentani and R. Brout, Nucl. Phys. B **388**, 474 (1992).
[40]D. L. Hill and J. A. Wheeler, Phys. Rev. **89**, 1102 (1953).
[41]K. W. Ford, D. L. Hill, M. Wakano, and J. A. Wheeler, Ann. Phys. **7**, 239 (1959).
[42]J. Ankerhold, H. Grabert, and G. Ingold, Phys. Rev. E **51**, 4267 (1995).
[43]Since the operators $\hat{\xi}$ and $\hat{\eta}$ remind us of the annihilation and creation operator, one might wonder if the states $|\xi\rangle$ and $|\eta\rangle$ play a similar role as the coherent states in the harmonic oscillator.[61] Indeed, their time evolution in the inverted harmonic oscillator takes the form $e^{-\omega t/2}|e^{-\omega t}\xi\rangle$ and $e^{\omega t/2}|e^{\omega t}\eta\rangle$, respectively. This dependency resembles the one[51] obtained for the time evolution $e^{-i\Omega t/2}|e^{-i\Omega t}\alpha\rangle$ of a coherent state $|\alpha\rangle$ in a harmonic oscillator of frequency Ω. It is interesting to note that coherent states have also been identified in other quantum systems as the free particle.[62] We postpone a detailed analysis of these particular states to a subsequent publication.
[44]D. Chruściński, J. Math. Phys. **44**, 3718 (2003).
[45]D. Chruściński, J. Math. Phys. **45**, 841 (2004).
[46]J. Twamley and G. J. Milburn, New J. Phys. **8**, 328 (2006).
[47]R. Hilfer, *Applications of Fractional Calculus in Physics* (World Scientific, Singapore, 2000).
[48]P. A. M. Dirac and R. H. Fowler, Proc. R. Soc. London, Ser. A **112**, 661 (1926).
[49]*NIST Digital Library of Mathematical Functions*, edited by F. W. J. Olver, A. B. Olde Daalhuis, D. W. Lozier, B. I. Schneider, R. F. Boisvert, C. W. Clark, B. R. Miller, B. V. Saunders, H. S. Cohl, and M. A. McClain, http://dlmf.nist.gov/, Version 1.1.5, release date 2022-03-15.
[50]E. Wigner, Phys. Rev. **40**, 749 (1932).
[51]W. P. Schleich, *Quantum Optics in Phase Space* (Wiley-VCH, Weinheim, 2001).
[52]G. G. Rozenman, M. Zimmermann, M. A. Efremov, W. P. Schleich, L. Shemer, and A. Arie, Phys. Rev. Lett. **122**, 124302 (2019).
[53]S. Feng and H. G. Winful, Opt. Lett. **26**, 485 (2001).
[54]M. Zimmermann, M. A. Efremov, A. Roura, W. P. Schleich, S. A. DeSavage, J. P. Davis, A. Srinivasan, F. A. Narducci, S. A. Werner *et al.*, Appl. Phys. B **123**, 102 (2017).
[55]O. Amit, Y. Margalit, O. Dobkowski, Z. Zhou, Y. Japha, M. Zimmermann, M. A. Efremov, F. A. Narducci, E. M. Rasel *et al.*, Phys. Rev. Lett. **123**, 083601 (2019).
[56]M. Zimmermann, "Interference of matter waves—Branch-dependent dynamics, the Kennard phase, and T^3 Stern-Gerlach interferometry," Ph.D. thesis (Ulm University, Ulm, 2021).
[57]R. Penrose, Found. Phys. **44**, 557 (2014).
[58]R. Howl, R. Penrose, and I. Fuentes, New J. Phys. **21**, 043047 (2019).
[59]W. Pauli, *Wave Mechanics: Volume 5 of Pauli Lectures on Physics* (Dover Publications Inc., Mineola, 2000).
[60]Y. Brychkov, O. Marichev, and N. Savischenko, *Handbook of Mellin Transforms* (Chapman and Hall/CRC, New York, 2018).
[61]V. V. Dodonov and V. I. Man'ko, "Invariants and the evolution of nonstationary quantum systems," in *Proceedings of the Lebedev Physics Institute of the Academy of Sciences of the USSR*, edited by M. A. Markov (Nova Science Publ., New York, 1989), Vol. 183.
[62]O. V. Man'ko and V. I. Man'ko, Entropy **23**, 549 (2021).